https://doi.org/10.5194/egusphere-2026-4521
Preprint. Discussion started: 7 August 2026

Otolith trace element composition reveals spatial and ontogenetic structuring in the glacier lanternfish *Benthosema glaciale* (Reinhardt, 1837)

Francesco Saltalamacchia[1,2], Natalya D. Gallo[1,2,3], Arild Folkvord[1,4], Anne Gro Vea Salvanes[1,2], Karin Limburg[5,6]

[1]Department of Biological Sciences, University of Bergen, Bergen, Norway
[2]Bjerknes Centre for Climate Research, Bergen, Norway
[3]Norwegian Research Centre (NORCE), Bergen, Norway
[4]Institute of Marine Research (IMR), Bergen, Norway
[5]Department of Environmental Biology, State University of New York College of Environmental Science and Forestry, Syracuse (New York), US
[6]Department of Aquatic Resources, Swedish University of Agricultural Sciences, Uppsala, Sweden

Correspondence to: Francesco Saltalamacchia (francesco.saltalamacchia@uib.no)

Abstract. Detecting habitat use in mesopelagic fishes is hampered by a lack of detailed surveys. Otolith chemistry can fill this gap by providing lifetime chronologies of the environmental conditions experienced by individuals. We analysed otolith transects of six trace elements with known environmental or physiological sensitivity in the dominant North Atlantic myctophid, the glacier lanternfish *Benthosema glaciale*. Fish were sampled across a complex fjord–shelf system where topographic and hydrographic conditions create vertical and horizontal structuring. Element:Ca ratios changed with age in all six elements. Overall, Sr increased through life, while Ba declined during juvenile stages and rose again in adults. These paired trajectories align with a shift from early exposure to surface-influenced waters toward longer residence in deeper water masses as fish grow. Mg and Mn were highest early in life and declined thereafter, suggesting ontogenetic control linked to growth and physiology. P increased from around the age of maturation, while B showed a weaker age structure. Spatial patterns were dominated by a contrast between the coastal site and the fjords, with additional element-specific differences among fjords. Individual fish also differed persistently in their overall elemental levels and in how their chemical trajectories changed with age. Several elements covaried after accounting for age, site and individual structure, most strongly Sr with Ba, suggesting shared incorporation processes or exposure histories beyond their common ontogenetic and spatial trends. Our results indicate that otolith chemistry in *B. glaciale* records life-stage-specific information on water-mass exposure, providing a retrospective window on habitat use where direct observation is impractical. More broadly, they highlight the value of this approach for linking biological and biogeochemical processes in deep and vertically structured systems.

https://doi.org/10.5194/egusphere-2026-4521
Preprint. Discussion started: 7 August 2026

1 Introduction

Ontogenetic niche shifts, i.e. changes in diet or habitat over an organism's life, are widespread among animals and reflect stage-specific physiological demands and trade-offs (de Roos et al., 2002). In fishes, conspicuous changes in size, morphology, and behaviour make ontogenetic habitat shifts particularly common (Persson and Crowder, 1998). These movements can occur horizontally between different habitats (coastal and open-sea, freshwater and marine), or vertically within the same system (changes in depth distribution) (Loutrage et al., 2024; Sánchez-Hernández et al., 2019).

The mesopelagic or twilight zone occupies about 20-30% of the total ocean volume (Proud et al., 2017; Reygondeau et al., 2018). Mesopelagic fishes are a key component of deep sound-scattering layers (dense aggregations of marine organisms detectable by echosounders) and undertake extensive diel vertical migrations (DVM) that support trophic linkages and carbon transport between productive surface waters and the deep sea (Saba et al., 2021). Because mesopelagic biogeochemical processing depends strongly on the depth distribution and activity of organisms, resolving ontogenetic shifts in habitat use remains an important challenge (Robinson et al., 2010). Moreover, although interest in mesopelagic organisms as potential fisheries resources has grown, major gaps remain in their life histories, population dynamics, trophic roles, and responses to oceanographic and climatic variability (Eduardo et al., 2021; Hidalgo and Browman, 2019; St. John et al., 2016).

Inferring habitat use in mesopelagic fishes is challenging due to the logistical constraints of sampling at depth and the difficulty of tracking small, fragile organisms. Trawl surveys provide only snapshots of population structure, integrated across depth layers and strongly influenced by short-term environmental conditions. Individual tracking through tagging or laboratory experiments has so far proven infeasible. These limitations are exacerbated in species exhibiting size- or season-dependent variation in the intensity or direction of DVM. Tools capable of retrospectively integrating depth-dependent environmental exposure across ontogeny are therefore particularly valuable.

An alternative approach to tagging is the use of fish earstones (otoliths) as “voyage recorders”. Otoliths are hard structures located in the inner ear of bony fishes, where they function as part of the hearing and balance systems. Sagittal otoliths (the largest of three pairs) are composed mainly of calcium carbonate in the form of aragonite precipitated on a protein matrix (Degens et al., 1969). However, they also include varying amounts of minor and trace elements (Campana, 1999), commonly distinguished by whether their concentrations are above or below 1000 ppm, respectively (Clarke and Sloss, 1992).

As metabolically inert structures that accrete throughout life, otoliths retain a permanent record of growth, with new material deposited proportionally to the individual’s physiological and metabolic activity (Morales-Nin, 2000). In many species, alternating translucent (slow growth) and opaque (fast growth) otolith phases arise from seasonal variation in the ratios of carbonate to organic matrix deposition, with each translucent–opaque pair typically representing one year of growth.

Beyond ageing applications, otoliths have been shown to serve as valuable natural tags, providing insights into the growth, population structure, and environmental history of fishes (Thorrold et al., 2001). Concentrations of minor and trace elements embedded into the incremental structure of the otolith may record changes in environmental conditions experienced by the

https://doi.org/10.5194/egusphere-2026-4521
Preprint. Discussion started: 7 August 2026

fish (e.g. water chemistry, salinity, oxygen, temperature) (Hüssy et al., 2022; Limburg et al., 2011; Thorrold et al., 1997) and/or physiological processes related to growth, sexual maturation and metabolism (Hüssy et al., 2020; Sturrock et al., 2015). Consequently, spatial and temporal variation in otolith chemistry has been widely used to infer aspects of habitat use, migration and past exposure to diverse physicochemical conditions (Gauthier et al., 2024; Limburg et al., 2015; Vrdoljak et al., 2020; Xuan et al., 2022).

Myctophids (lanternfishes) dominate the mesopelagic zones of the world's oceans (Catul et al., 2011). In the North Atlantic, the most abundant species in this family is the glacier lanternfish *Benthosema glaciale* (Reinhardt, 1837) (Gjøsaeter and Kawaguchi, 1980), occurring in both open waters and semi-enclosed systems such as deep fjords. Along the Norwegian coast, fjord topography creates pronounced vertical gradients in salinity, oxygen, and water chemistry (Meyer et al., 2020; Skei and Melsom, 1982; Syvitski et al., 2012), while also supporting high densities of mesopelagic fishes (Giske et al., 1990; Salvanes et al., 2025).

Abundant, semi-isolated subpopulations of *B. glaciale* have been identified in these fjords (Kristoffersen and Salvanes, 2009; Quintela et al., 2024; Suneetha and Salvanes, 2001). Acoustic studies in this region have shown that, despite limited horizontal movements, *B. glaciale* undergo ontogenetic changes in depth distribution, with individuals generally occupying deeper waters after sexual maturation and exhibiting size-dependent and seasonal DVM patterns (Dypvik et al., 2012b). These observations provide an important ecological framework for interpreting otolith chemical records and applying them to advance understanding of the species' ecology.

Recent work using otolith shape and age-resolved microchemistry in *B. glaciale* suggested that connectivity among adjacent fjords may be greater during early life stages and weaker later in ontogeny, based on overlapping elemental signatures in early life and a weak tendency toward increasing divergence at older ages (Saltalamacchia et al., 2026). This raises the question of whether age-related changes in otolith chemistry are consistent with ontogenetic shifts in habitat use and environmental exposure, and whether these chemical records can reveal patterns of depth use and residency that cannot be resolved from snapshot observations of scattering layers or trawl catches.

In this study, we use otolith microchemistry to examine how elemental concentrations in *B. glaciale* vary across ontogeny and reflect environmental conditions at the fjord scale, interpreting these patterns in the context of local hydrographic structure. We focus on isotopes identified as potential environmental or physiological tracers in marine fish (Hüssy et al., 2020; Limburg et al., 2023): ^{88}Sr, ^{138}Ba, ^{11}B, ^{25}Mg, ^{55}Mn, ^{31}P. These elements span a spectrum of environmental and physiological sensitivities, allowing complementary aspects of habitat use, water-mass exposure and internal state to be assessed throughout life.

In marine waters, strontium (Sr) is supplied primarily by continental weathering delivered by rivers (Palmer and Edmond, 1989). Although growth-related effects may also modulate the signal (Hüssy et al., 2020; Sturrock et al., 2015), otolith Sr is mostly considered an environmental tracer because its incorporation tends to reflect ambient concentrations (Campana, 1999; Walther and Limburg, 2012). These are typically low in freshwater and higher and more stable in marine systems (Hüssy et al., 2020). Sr is therefore widely used to trace marine influence and movements across salinity gradients (Hüssy et

https://doi.org/10.5194/egusphere-2026-4521
Preprint. Discussion started: 7 August 2026

al., 2020) and, in vertically structured systems, relative depth or water-mass exposure (Wu et al., 2024). In *B. glaciale*, otolith Sr would be expected to increase through ontogeny if fish progressively deepen from shallower, coastally influenced habitats into deeper and more marine water masses.

Otolith barium (Ba) is also generally treated as an environmental tracer with incorporation reflecting ambient concentrations (Hüssy et al., 2020). In coastal waters, Ba often reflects a combination of terrestrial inputs, biological cycling, and regeneration at depth, resulting in nutrient-like behaviour characterised by depletion in productive surface layers and enrichment in deeper, upwelled or anoxic waters (Bath et al., 2000; Guay and Kenison Falkner, 1997; Walther et al., 2013; Walther and Limburg, 2012). Accordingly, Ba is expected to vary across ontogeny if individuals shift between water masses with contrasting Ba availability. Additional differences among fjords may also occur, potentially including higher Ba in more isolated basins where terrestrial influence is stronger and exchange with coastal waters is restricted (Brinkmann et al., 2022).

Otolith boron (B) is less established than Sr or Ba, but available evidence suggests that it may respond to water carbonate chemistry, acid–base regulation and growth processes, with higher B in foraminifer shells generally associated with higher seawater pH (Yu et al., 2007). Recent studies in cod have linked lower otolith B to lower pH and lower dissolved oxygen (Limburg et al., 2023).

Otolith magnesium (Mg) is generally interpreted as a physiologically mediated tracer, with incorporation rates considered to be mostly linked to metabolic activity and growth rather than external water chemistry alone (Hüssy et al., 2020; Limburg et al., 2018; Limburg and Casini, 2019). Accordingly, Mg is expected to be highest early in life and decline through ontogeny as metabolism and somatic growth decrease, broadly following an inverse growth trajectory (Limburg et al., 2018).

Manganese (Mn) is supplied to coastal waters by riverine input and is further mobilised under low-oxygen, reducing conditions (Limburg et al., 2015). Its availability is therefore often enhanced in restricted deep basins and inner-fjord environments relative to well-ventilated outer fjords and coastal waters (Brinkmann et al., 2023; Hamilton-Taylor and Price, 1983). In otoliths, Mn is influenced not only by ambient availability but also by growth and metabolism-related processes, which complicates its interpretation as a purely environmental tracer (Cavole et al., 2023; Turner and Limburg, 2015). In *B. glaciale*, ontogenetic deepening would therefore be expected to produce an overall decline in otolith Mn if juveniles spend more time in shallower or more coastally influenced waters and adults increasingly occupy deeper layers where dissolved Mn is generally low. However, this pattern could weaken in more isolated fjords where restricted ventilation and redox recycling may maintain elevated Mn at depth (Brinkmann et al., 2023; Hamilton-Taylor and Price, 1983).

Finally, otolith phosphorus (P) is generally treated as a physiologically mediated tracer because it is thought to be closely linked to the organic matrix and biomineralisation (Hüssy et al., 2020). Available evidence suggests that P can vary with matrix synthesis and growth-related processes, but the exact mechanisms and expected ontogenetic trajectory remain poorly resolved (Hüssy et al., 2020). We therefore included P as a complementary tracer of internal, possibly life-stage-related change.

https://doi.org/10.5194/egusphere-2026-4521
Preprint. Discussion started: 7 August 2026

By interpreting otolith chemical signatures in the context of known ontogenetic behaviour and fjord hydrography, this study aims to clarify how mesopelagic fishes exploit vertically structured environments, and how otolith chemistry can be used to infer habitat use in deep-water species for which direct monitoring remains logistically challenging.

Specifically, we ask: (1) how otolith elemental composition in *B. glaciale* is structured across ontogeny; (2) whether age-related patterns in elements with known environmental dependency, particularly Sr and Ba, are consistent with expected shifts in depth-related habitat use and water-mass exposure across development; and (3) whether elements with different sensitivities to environmental exposure and physiological processes covary within and among individuals, indicating shared incorporation processes or persistent differences integrated across life.

A further aim is to provide a first description of ontogenetic trace-element variation in *B. glaciale*, given that the mechanistic basis of several otolith tracers remains incompletely understood, and may vary, among taxa and systems.

2 Material and methods

2.1 Study species

Benthosema glaciale is a zooplanktivorous fish primarily feeding on copepods (Knutsen et al., 2023). Individuals attain a maximum length of ~80 mm, reach sexual maturity between the ages of 2 and 3 (Gjøsæter, 1981; Halliday, 1970), and live for up to 8 years (Gjøsæter, 1973). Growth rates vary on regional and local scales (Halliday, 1970; Kristoffersen and Salvanes, 2009; Vastenhoud et al., 2023).

Acoustic and trawl studies in Masfjord show that vertical habitat use in *B. glaciale* varies with body size, season and time of day. Larger individuals occur deeper than smaller ones, and fish below ~250–300 m are mainly older juveniles and adults (Dypvik et al., 2012a, b). This depth structure has been interpreted as a trade-off between faster growth and feeding opportunities in shallower, more illuminated waters and lower predation risk at depth, where visual feeding is more difficult. Seasonal DVM patterns further change the depths occupied during otolith formation. During spring and summer, part of the population performs “normal” DVM, descending to deep water during daytime and ascending toward shallower layers at night, while a deep non-migrating component remains present throughout the year (Dypvik et al., 2012b). During autumn and winter, deep-living fish more often remain at depth or perform inverse DVM (Dypvik et al., 2012b). In autumn, inversely migrating age-2 and older fish occupied ~200–270 m in Masfjord during daytime, fed on overwintering Calanus, and descended below ~270 m at night (Dypvik et al., 2012a).

Otolith increment validation in *B. glaciale* was first carried out by Gjøsæter (1970). Along the Norwegian coast, translucent (slow-growth) increment deposition is known to occur during the spring and summer months (March to September, overlapping the spawning season), while opaque (fast-growth) deposition is typically dominant during autumn and winter (Gjøsæter, 1973). For the otolith record, the varying DVM behavioural patterns mean that translucent and opaque increments are unlikely to represent simple arithmetic averages across all depths visited during diel migration. The chemical signal likely integrates the water masses occupied during the period of otolith accretion, with stronger influence from depths

https://doi.org/10.5194/egusphere-2026-4521
Preprint. Discussion started: 7 August 2026

and times where growth, feeding and biomineralisation are greatest. In spring–summer, when translucent material is expected to form, the signal may combine deep daytime residence with shorter night-time excursions into shallower layers. In autumn–winter, when opaque material forms, the signal in older fish can be expected to be more influenced by deep and mid-water habitats, including daytime feeding depths during inverse DVM and deeper night-time or non-migrating depths.

2.2 Sampling and processing of otoliths

Fish were sampled through pelagic trawling across a fjord–shelf system on the Norwegian west coast, spanning an exposed coastal site and five fjord basins (Fig. 1). These sites differ in sill depth, basin depth, catchment area size and degree of exchange with coastal water (Saltalamacchia et al., 2026), capturing a gradient from well-ventilated to more weakly renewed fjord basins. Sogndalsfjord (SOG) represents a shallow-silled basin (25 m deep sill, 260 m maximum depth) connected to the larger Sognefjord (Paetzel and Dale, 2010). The coastal site (COA) lies north of Sognefjord's mouth and has a bottom depth of 380 m. The Fensfjord system includes a deep, well-connected basin (FEN, sill depth ~380 m) and Masfjord, an adjacent shallow-silled branch (MAS, sill depth ~ 75 m); the two basins have maximum depths of 680 and 490 m, respectively (Hjelstuen et al., 2013; Kaartvedt et al., 1988), and oxygen levels in the deep basin of MAS have been decreasing over the past decades, becoming near-hypoxic between 2016 and 2021 (Aksnes et al., 2019; Salvanes et al., 2025). Two additional fjords, Osterfjord (OST) and Sørfjord (SØR), with maximum depths of 650 and 400 m respectively, belong to the estuarine system east of Bergen, where exchange with the outer coast is constrained by multiple sills (Helle, 1978).

The trawl catches were sorted and processed as described by Salvanes et al. (2018), and randomly selected individuals were stored frozen until otolith extraction. Sagitta otoliths were extracted under a dissection microscope and rinsed in distilled water. After covering the otoliths in distilled water to enhance the increment visibility, photographs of each pair were taken under reflected light against a dark background (Fig. 2a). Age determination was carried out using digital images of both otoliths in a pair. We then selected one otolith per fish using a binary random-number generator. The otoliths were weighed, embedded in epoxy resin, and sectioned longitudinally through their cores using a low-speed saw with 0.3 mm diamond wafering blades and a 1-mm separator. Sections were polished with a silicon carbide grinding paper, rinsed in distilled water and mounted on glass microscope slides.

https://doi.org/10.5194/egusphere-2026-4521
Preprint. Discussion started: 7 August 2026

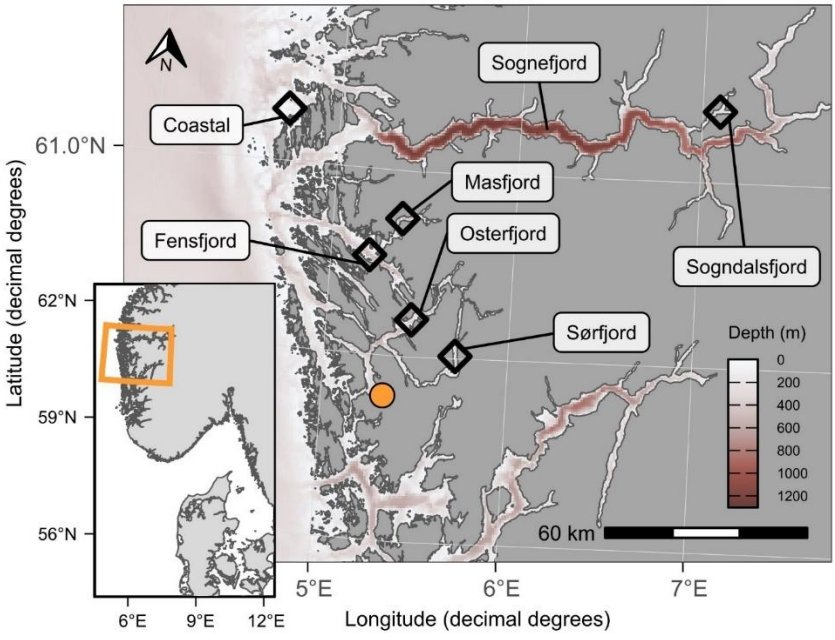

Figure 1 Sampling area along the Norwegian west coast for the study of otolith microchemistry of *Benthosema glaciale*. The sampling sites are indicated by open diamonds on the main map. From west to east: Coastal (abbreviated as COA throughout the manuscript), Fensfjord (FEN), Masfjord (MAS), Osterfjord (OST), Sørfjord (SØR), Sogndalsfjord (SOG). The position of the city of Bergen is highlighted by a circle, for orientation. From: Saltalamacchia et al. (2026).

2.2.1 Acquisition and processing of trace element data

Using a Triple Quadrupole ICP-MS (iCAP TQ ICP-MS) connected to a Teledyne-Photon Analyte Excite+ excimer laser (193 nm wavelength), we ran edge-to-edge transects (ablation points) along the major otolith growth axis and passing through the core (Fig. 2). All transects were pre-ablated to clean the surface (laser fluence 0.81 J·cm^{-2}) and then ablated (1.62 J·cm^{-2}) at a constant travel speed of 3 µm·s^{-1} with a spot size of 50 µm. A micro-analytical phosphate standard (MAPS4, U.S. Geological Survey) was ablated (fluence 2.03 J·cm^{-2}) at the beginning of each session and every 7-10 otolith transects to calibrate the conversion from count per second (cps) to part per million (ppm) and correct for machine drift. Ambient elemental concentrations were acquired for 30 seconds prior to each ablation. Using the software Iolite v. 4.10.1 (Paton et al., 2011), the background signal was subtracted from each transect, and all measurements were converted from cps to ppm. The data were then imported into R for further processing.

All selected elements (Sr, Ba, B, Mg, Mn, P) had more than 85% measurements above their respective limit of detection (LOD) (Longerich et al., 1996). Below-LOD values were corrected within each element and transect using linear interpolation between the closest measurements on each side. Across all transects, ~4% of points required adjustment (below LOD or visually implausible artefacts). Finally, element concentrations were converted to element-to-calcium ratios (E:Ca^{43}) times 10^5. Further details on instrument settings, calibration procedures, and data-reduction workflows are provided in Saltalamacchia et al. (2026).

https://doi.org/10.5194/egusphere-2026-4521
Preprint. Discussion started: 7 August 2026

2.2.2 Measurement of otolith growth zones and alignment with elemental profiles

After ablation, each section was covered with glycerol to enhance the visibility of the otolith macrostructure and the laser path, and then photographed under reflected light (Fig. 2b). Distance along each laser path was measured in ImageJ v. 1.52p (Schneider et al., 2012) between the ventral margin and the otolith core, and subsequently at each opaque/translucent transition between the core and the dorsal margin (Fig. 2b, Fig. 3). We used only elemental concentrations acquired on the dorsal side, as increments were clearer and therefore more suitable for accurate measurements. Furthermore, because the narrow otolith cores were less likely to have been sectioned consistently across individuals, we focused our analyses on the subsequent growth phases. Based on its position along the laser path, each ablation point was assigned to a specific growth phase (translucent or opaque), nominal age class, and year of formation.

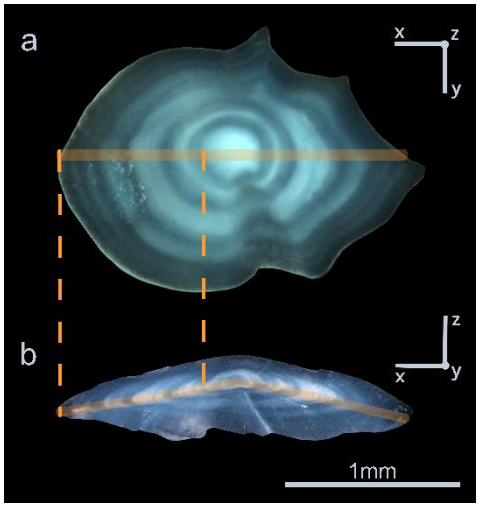

Figure 2 Annotated views of a left sagitta otolith of *B. glaciale* collected in Masfjord, Norway. (a) Top view used for age determination, with the sectioning plane highlighted. (b) Longitudinal section used for microchemical analysis, showing the edge-to-edge laser ablation path and the otolith portion analysed in this study (vertical lines). Three-dimensional Cartesian axes illustrate viewing orientation (x: dorso-ventral; y: antero-posterior; z: transverse). Modified from: Saltalamacchia et al. (2026).

Table 1 Summary of the samples included in the study of otolith microchemistry of *B. glaciale*. Site: sampling location. Abbreviation: short notation for each site, adopted throughout the manuscript. For each site, the total number of ablation points across all fish, the minimum and maximum continuous age (as defined in the "Statistical analysis" section), the mean continuous age ± standard deviation, and the range of years during which the increments were formed are also provided.

			Ablation points			
Site	**Abbreviation**	**N. fish**	**N. points**	**Age range**	**Mean age**	**Year range**
Coastal	COA	6	548	0.0-5.9	2.2 ± 1.2	2013-2021
Fensfjord	FEN	24	1753	0.0-5.9	2.0 ± 1.1	2015-2021
Masfjord	MAS	41	2928	0.0-5.9	2.2 ± 1.2	2013-2021

https://doi.org/10.5194/egusphere-2026-4521
Preprint. Discussion started: 7 August 2026

			Ablation points			
Site	**Abbreviation**	**N. fish**	**N. points**	**Age range**	**Mean age**	**Year range**
Osterfjord	OST	24	1533	0.0-5.9	2.2 ± 1.2	2013-2020
Sogndalsfjord	SOG	7	488	0.0-5.5	2.1 ± 1.1	2016-2021
Sørfjord	SØR	8	548	0.0-5.5	2.4 ± 1.2	2015-2020

2.3 Statistical analysis

2.3.1 Ontogenetic trajectories in trace element incorporation

We modelled otolith element:Ca ratios (E:Ca; E = Sr, Ba, B, Mg, Mn, P) separately for each element using hierarchical Generalised Additive Mixed Models (GAMMs). GAMMs were used because E:Ca relationships with age were strongly nonlinear and because each fish contributed repeated measurements across the otolith transect. Model construction followed the workflow described by Ng et al. (2025), adapted to our data structure and research questions. Models were fitted using the *bam()* function from the *mgcv* package in R (Wood, 2001).

Each laser ablation point was assigned a continuous age based on its position within otolith growth increments. Translucent increments were assumed to represent 58% of a year (March–September) and opaque increments 42% (October–February), following observations for fish aged ≥ 1 in west-Norwegian fjords (Gjøsæter, 1973). For example, a point halfway through a translucent increment formed at age 3 was assigned age 3.29, while a point halfway through the following opaque increment was assigned age 3.79. For age-0 fish, where the patterns of deposition of optically distinct bands are less clearly defined and highly dependent on the time of spawning, translucent and opaque material were assigned equal duration. To maximise overlap among sites, analyses were restricted to increments formed between 2013 and 2021 and to otolith ages < 6 years (Table 1).

The central ecological expectation guiding the analysis was that otolith chemistry changes as fish grow because individuals undergo ontogenetic shifts in habitat use and physiology. We first fitted a shared smooth effect of age, with age centred at 2.00 years because this was close to the mean age of analysed otolith points and to the expected onset of maturation. We then added individual-level random intercepts and age slopes, allowing fish to differ in both overall element levels and in how E:Ca changed through life.

Spatial structure was then evaluated through alternative formulations of site effects. Specifically, we tested whether otoliths from different sites differed in average E:Ca, whether the age trajectory itself varied among sites, and whether E:Ca trajectories were better described as site-specific deviations from a shared population-level age curve or as fully site-specific trajectories reflecting finer-scale processes. Site-specific age trajectories were fitted either as factor-smooth interactions, where sites have the same allowed curve complexity, or as thin-plate smooths, where each site can have a different degree of complexity (Ng et al., 2025; Pedersen et al., 2019). In contrast to factor-smooth interactions, thin-plate smooths do not

https://doi.org/10.5194/egusphere-2026-4521
Preprint. Discussion started: 7 August 2026

include group-level intercepts by default. While such differences can be modelled as random effects (Pedersen et al., 2019), we included site as a fixed effect in this formulation to explicitly estimate overall site-level offsets in E:Ca after accounting for ontogenetic effects. Each formulation was fitted with and without a shared population-level age smooth, allowing us to test whether site trajectories were best described as deviations from a common pattern or as fully site-specific age trajectories (Ng et al., 2025). Throughout the workflow, model support was assessed using Akaike's Information Criterion (AIC), with the simpler formulation preferred when $\Delta AIC < 2$.

Temporal structure was modelled using a sequential growth-season index capturing both seasonality and long-term environmental drift. This index followed the order of translucent and opaque deposition phases across years (e.g. translucent 2013, opaque 2013, translucent 2014, etc.). We compared a random intercept shared across sites with a growth-season × site random intercept, allowing temporal offsets to differ among sites.

All E:Ca ratios were positive and right-skewed, so we used models with a Gamma error distribution and a log link. Smoothing parameters were estimated by restricted maximum likelihood (fREML). Basis dimensions (the upper limit on smooth complexity) were initially set to k = 15, slightly above twice the number of age classes, and reduced when needed for convergence. Model adequacy was checked using effective degrees of freedom, k-index diagnostics (Pedersen et al., 2019), concurvity diagnostics and residual plots. The selected spatial structure for each element and the corresponding final model formulation, including individual and temporal random effects, are summarised in Table 2; the full candidate model set is provided in Appendix A (Table A1). Final models were used to generate marginal predictions of age-specific E:Ca trajectories for visualisation.

Table 2 Selected GAMM structures for element-specific otolith E:Ca trajectories. All candidate models are provided in Table A1. The table reports the retained spatial structure ("Selected model") for each element group ("E:Ca"). In the model formulations, η is the expected response under a log-link, β_0 is the intercept, site is a categorical fixed effect, f(age) is a shared age smooth, f_s(age) is a site-specific thin-plate age smooth, g_s(age) is a site-specific factor smooth. All selected models also included individual-level random intercepts and age slopes (b_i, b_i(age)), as well as a growth-season × site random effect (b_{ts}) allowing temporal offsets to differ among sites (m3b temporal formulation in Table A1).

Selected model	E:Ca	Full model formulation	Model rationale
$m2_e$	Sr:Ca, Mg:Ca	$\eta = \beta_0 + site + f_s(age) + b_i + b_i(age) + b_{ts}$	No common age trend: each site has its own age-related chemical trajectory, with site trajectories allowed to differ in complexity. A fixed site term estimates overall site-level offsets in E:Ca.
$m2_d$	Ba:Ca	$\eta = \beta_0 + f(age) + site + f_s(age) + b_i + b_i(age) + b_{ts}$	A common ontogenetic trend is retained and modulated by site-specific deviations, with site trajectories allowed to differ in complexity. A fixed site term estimates

https://doi.org/10.5194/egusphere-2026-4521
Preprint. Discussion started: 7 August 2026

			overall site-level offsets in E:Ca.
$m2_c$	B:Ca, Mn:Ca, P:Ca	$\eta = \beta_0 + g_s(age) + b_i + b_i(age) + b_{ts}$	No common age trend: each site has its own age-related chemical trajectory, with all site trajectories fitted under the same smoothness constraint.

2.3.2 Covariation in trace element incorporation

While univariate GAMMs describe how single elements vary with ontogeny, space and time, elements are incorporated simultaneously within the otolith and may therefore respond to shared environmental conditions or physiological processes. Because all the analysed elements show strong age-related and spatial structure, simple correlations among raw values would largely reflect parallel trends rather than genuine covariation. To assess whether element pairs exhibit coordinated patterns of incorporation in *B. glaciale*, we fitted a multivariate mixed-effects model using *MCMCglmm* (Hadfield, 2010) based on Grammer et al. (2017). This approach allows the separation of short-term covariation within individuals from persistent, life-integrated differences among fish after accounting for shared age, site, and individual effects (Grammer et al., 2017). Given the univariate results, increments formed before age 2 were excluded to minimise early-life variability associated with shallow-water environments.

The model was fitted using weakly informative priors and three independent MCMC chains (110,000 iterations, 10,000 burn-in, thinning = 25). Log-transformed and standardised E:Ca ratios were analysed jointly as Gaussian traits, with the continuous age predictor log-transformed and centred at 2.00 to improve interpretability and convergence. The model estimated element-specific intercepts, age effects, and site effects, while fish identity was included as a random effect with an unstructured variance-covariance matrix across traits. Convergence was assessed using trace plots, effective sample sizes, autocorrelation diagnostics, and Gelman–Rubin $\hat{R}$ statistics.

We then used posterior variance–covariance estimates to calculate among- and within-individual (residual) co-variation between element pairs after accounting for fixed and random effects, with significance based on whether 95% credible intervals excluded zero (Grammer et al., 2017). The within-individual matrix describes whether element concentrations rise and fall together over the life course. Positive correlations at this level indicate that deviations in one element coincide with deviations in another, consistent with short-lived environmental events or transient physiological responses. The among-individual matrix describes how elements covary based on their life-integrated average levels. Positive correlations indicate that individuals with above-average concentrations of one element also tend to be above average on another, suggesting shared long-term influences such as persistent habitat use or stable physiological profiles. These matrices allow inference about whether elements are linked primarily through short-term fluctuations within individuals, persistent life-integrated differences, both, or neither.

https://doi.org/10.5194/egusphere-2026-4521
Preprint. Discussion started: 7 August 2026

3 Results

The width of growth increments measured from the otolith sections of *B. glaciale* (110 fish, 985 increments; Table 1) increased from age class 0 to 1, and then decreased with age (Fig. 3). After the second year of life, translucent and opaque increments were similar in width. The average number of laser ablation points per translucent and opaque increments was, respectively, 4-9 at age 0; 6-23 at age 1; 6-10 at age 2; 4-6 at age 3; 4-4 at age 4; and 3-4 at age 5.

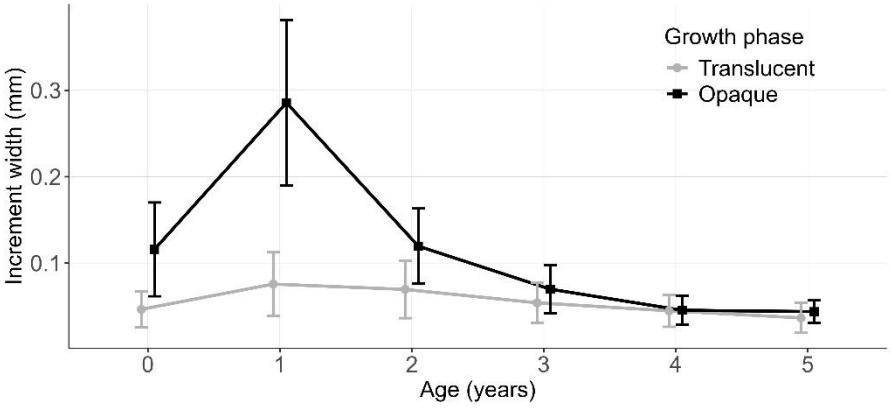

Figure 3 Average width (mm) ± standard deviation of otolith increments from all *B. glaciale* included in the present study. Measurements were taken at each growth phase transition (translucent-opaque) from longitudinal sections spanning the distance between the outer edge of the core and the dorsal margin. Note: age 0 increments (translucent and opaque) are those deposited just outside the core during the year of hatching.

3.1 Ontogenetic trajectories in trace element incorporation

Element:Ca ratios (E:Ca) changed with age in all six elements (Fig. 4). Otolith strontium (Sr:Ca), phosphorus (P:Ca) and, in most sites, boron (B:Ca) tended to increase through life. Magnesium (Mg:Ca) and manganese (Mn:Ca) were highest early in life and then declined. Barium (Ba:Ca) declined through juvenile stages and increased again in adults. The coastal site often differed from the fjord sites, which were usually more similar to one another, although element-specific differences remained among fjords as well. For all elements, the models supported persistent individual differences in both average E:Ca and the shape of age trajectories. Growth-season × site effects were also retained in the final models for all elements (Table 3, Table 4).

https://doi.org/10.5194/egusphere-2026-4521
Preprint. Discussion started: 7 August 2026

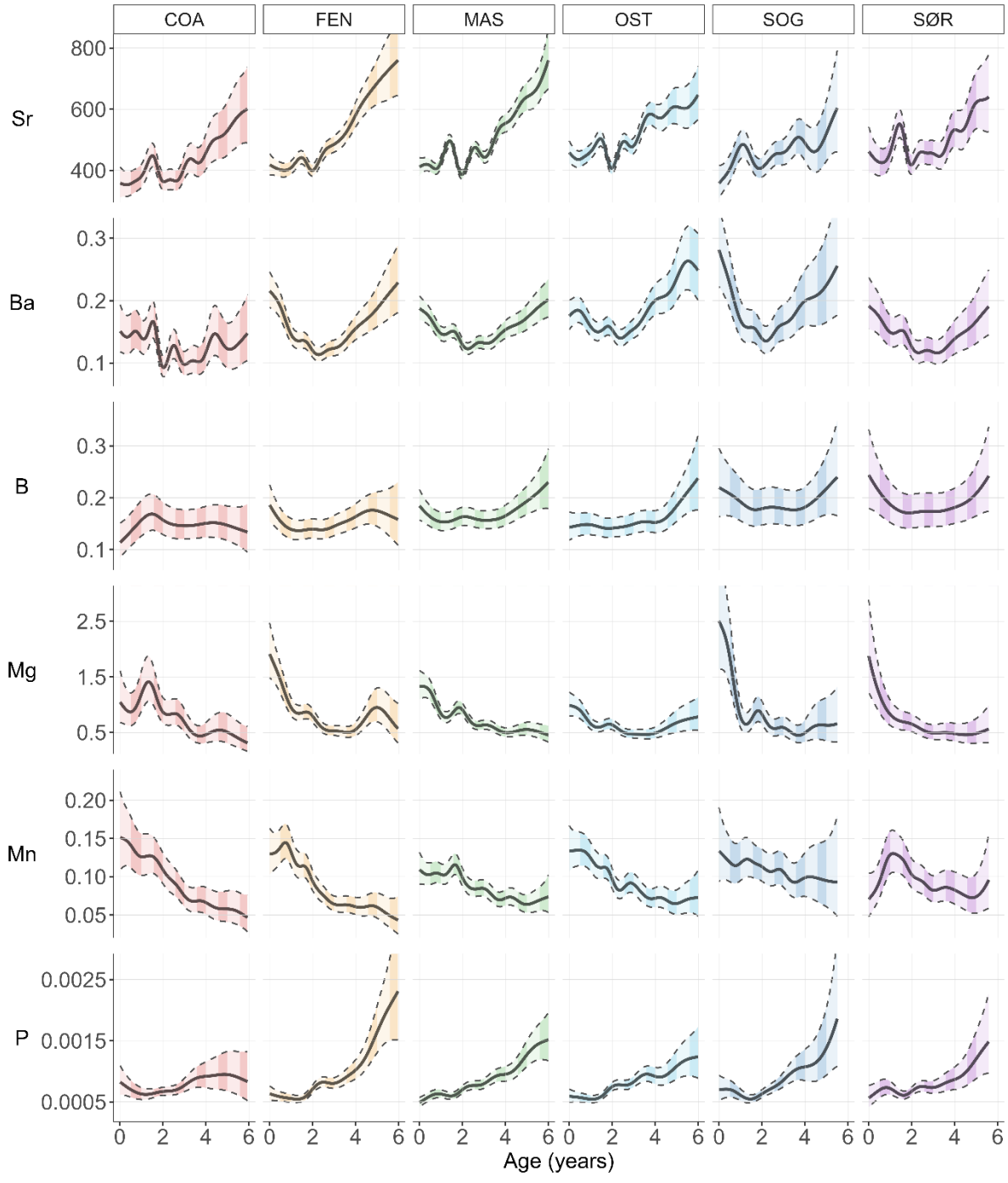

325 **Figure 4 Predicted age trajectories of trace element incorporation (Element [ppm]:Ca [ppm] · 10^5) from otoliths of *B. glaciale*. Each column represents one of the six sampling sites along the Norwegian west coast. Solid lines show population-level model predictions and shaded ribbons indicate 95% confidence intervals. Background shading denotes alternating translucent (lighter) and opaque (darker) otolith growth phases mapped onto continuous age.**

https://doi.org/10.5194/egusphere-2026-4521
Preprint. Discussion started: 7 August 2026

Sr:Ca increased with age after a dip around ages 1–2 (Fig. 4). At the reference age of 2.00, Sr:Ca was lower at the coastal site (COA) than in Fensfjord (FEN), Masfjord (MAS), Osterfjord (OST) and Sørfjord (SØR); Sogndalsfjord (SOG) was intermediate and not clearly different from COA (Table 3). Fjord trajectories generally reached higher adult Sr:Ca than the coastal site. Sub-annual oscillations consistent with the alternation of growth increments are visible across much of the trajectory, with a tendency to smooth down in later ages (Fig. 4). For Sr:Ca, the most supported model supported site-specific age trajectories of varying complexity ($m2_e$; Table 3).

Ba:Ca showed a U-shaped age trajectory. It declined from early life to a minimum around ages 2–3, then increased again in adults (Fig. 4). COA showed a weaker increase in adults than at the fjord sites. Among those, SOG had the highest Ba:Ca in both early and late life. Subannual oscillations are also more pronounced at COA than in fjords (Fig. 4). The selected model for Ba:Ca retained a shared age trajectory with site-specific deviations from a common population-wide trajectory ($m2_d$; Table 3).

B:Ca showed weaker age structure than Sr:Ca or Ba:Ca (Fig. 4, Table 3). The coastal trajectory increased during juvenile life and then remained relatively stable. In the fjords, B:Ca was mostly flat through early life and tended to increase in older fish. The B:Ca trajectory recorded in FEN resembles an intermediate pattern between COA and the inner fjords (Fig. 4). The selected model supported site-specific age trajectories with shared complexity ($m2_c$, Table 3).

Table 3 Summary of GAMM results from the retained models describing individual, spatial, temporal and ontogenetic variation in Sr:Ca, Ba:Ca and B:Ca from otoliths of *B. glaciale*. The retained spatial structure for each element is shown in brackets after the element symbol. All models also included individual-level random intercepts and age slopes, as well as the growth-season × site random effect. Top: fixed-effect estimates for site-level offsets; bottom: smooth-term statistics (effective degrees of freedom, EDF; F-values; p-values) for global age trends, site-specific ontogenetic deviations, individual-level random effects, and growth season × site structure. Estimates are reported on the log scale. In models with explicit fixed-site effects ($m2_d$, $m2_e$), the intercept is the reference-level model intercept for COA on the log scale, and site coefficients are log-scale offsets from COA. In models without a fixed site-offset term, the intercept is common across sites because site-level differences are represented within the site-specific age smooths. EDF gives the effective degrees of freedom for each smooth term and should not be interpreted as variance explained or an effect size: values near 1 indicate an approximately linear relationship, while larger values indicate a more nonlinear age structure. Site abbreviations: COA: Coastal; FEN: Fensfjord; MAS: Masfjord; OST: Osterfjord; SOG: Sogndalsfjord; SØR: Sørfjord.

	Sr:Ca [$m2_e$]			**Ba:Ca** [$m2_d$]			**B:Ca** [$m2_c$]		
	Estimate	**SE**	**P**	**Estimate**	**SE**	**P**	**Estimate**	**SE**	**P**
(Intercept)	5.996	0.039	< 0.001	-2.087	0.085	< 0.001	-1.796	0.063	< 0.001
SiteFEN	0.120	0.045	0.007	0.114	0.096	0.237			
SiteMAS	0.118	0.043	0.006	0.154	0.092	0.095			
SiteOST	0.171	0.045	< 0.001	0.279	0.096	0.004			
SiteSOG	0.095	0.054	0.078	0.301	0.117	0.010			
SiteSØR	0.155	0.053	0.003	0.116	0.114	0.306			
	EDF	**F value**	**P**	**EDF**	**F value**	**P**	**EDF**	**F value**	**P**
s(Age)				11.53	389.03	< 0.001			

https://doi.org/10.5194/egusphere-2026-4521
Preprint. Discussion started: 7 August 2026

	Sr:Ca [$m2_e$]			**Ba:Ca** [$m2_d$]			**B:Ca** [$m2_c$]		
	Estimate	**SE**	**P**	**Estimate**	**SE**	**P**	**Estimate**	**SE**	**P**
s(Age, Site)							29.58	276.60	0.036
s(Age):SiteCOA	10.74	346.42	< 0.001	11.98	100.43	0.151			
s(Age):SiteFEN	10.39	2310.36	< 0.001	6.63	71.60	0.164			
s(Age):SiteMAS	13.20	3009.99	< 0.001	0.00	0.00	0.018			
s(Age):SiteOST	11.98	945.53	< 0.001	9.75	206.55	0.014			
s(Age):SiteSOG	9.14	114.27	0.015	5.09	62.11	0.159			
s(Age):SiteSØR	11.23	193.95	0.006	3.51	26.38	0.337			
s(FishID)	99.51	70.73	< 0.001	102.00	161.62	< 0.001	102.96	81.90	< 0.001
s(FishID, Age)	93.15	34.39	< 0.001	95.81	65.57	< 0.001	88.19	16.80	< 0.001
s(Season x Site)	47.68	13.65	< 0.001	51.14	18.83	< 0.001	51.31	15.08	< 0.001

Mg:Ca was highest early in life and declined with age at all sites (Fig. 4). The decline was strongest during the first 1–2 years, after which trajectories became flatter. The coastal site showed a pronounced juvenile peak around age 1. At the reference age, average Mg:Ca in the fjords was not different than that at COA, except for OST, where it was lower (Table 4). As for Sr:Ca, the selected model for Mg:Ca supported site-specific age trajectories of varying complexity ($m2_e$; Table 4).

Mn:Ca also declined with age, broadly matching the Mg:Ca pattern (Fig. 4). The coastal site had high early-life Mn:Ca, followed by a steep decline. Except FEN and OST, fjord trajectories tended to lower initial levels and slower declines. The selected model supported site-specific age trajectories with shared complexity ($m2_c$, Table 4).

P:Ca was relatively flat during early life and increased from about age 2 in the fjords (Fig. 4). This increase was less evident at the coastal site, where P:Ca remained comparatively flat and reached lower values in older fish. Among fjords, trajectories were broadly similar in shape (i.e. showing increases with age). The selected model supported site-specific age trajectories with shared complexity ($m2_c$, Table 4).

These univariate models describe how each element changed with age and site. They do not estimate whether elements show coordinated incorporation after accounting for age, site, and individual trajectories. We therefore extended our analysis using multivariate mixed-effects models to test for covariation, consistent with shared environmental exposure or physiological control.

Table 4 Summary of GAMM results from the retained models describing individual, spatial, temporal and ontogenetic variation in Mg:Ca, Mn:Ca and P:Ca from otoliths of *B. glaciale*. The table follows the same structure as Table 3.

	Mg:Ca [$m2_e$]			**Mn:Ca** [$m2_c$]			**P:Ca** [$m2_c$]		
	Estimate	**SE**	**P**	**Estimate**	**SE**	**P**	**Estimate**	**SE**	**P**
(Intercept)	-0.166	0.127	0.191	-2.298	0.056	< 0.001	-7.253	0.044	< 0.001
SiteFEN	-0.086	0.146	0.558						

https://doi.org/10.5194/egusphere-2026-4521
Preprint. Discussion started: 7 August 2026

	Mg:Ca [$m2_c$]			**Mn:Ca** [$m2_c$]			**P:Ca** [$m2_c$]		
	Estimate	**SE**	**P**	**Estimate**	**SE**	**P**	**Estimate**	**SE**	**P**
SiteMAS	-0.077	0.140	0.582						
SiteOST	-0.338	0.145	0.020						
SiteSOG	-0.096	0.176	0.583						
SiteSØR	-0.260	0.171	0.129						
	EDF	**F value**	**P**	**EDF**	**F value**	**P**	**EDF**	**F value**	**P**
s(Age)									
s(Age, Site)				54.69	739.35	< 0.001	43.70	3412.56	< 0.001
s(Age):SiteCOA	7.96	810.11	< 0.001						
s(Age):SiteFEN	8.14	2146.62	< 0.001						
s(Age):SiteMAS	8.32	3241.75	< 0.001						
s(Age):SiteOST	7.13	475.57	0.002						
s(Age):SiteSOG	7.46	625.98	< 0.001						
s(Age):SiteSØR	5.66	554.78	0.002						
s(FishID)	100.40	95.89	< 0.001	103.76	117.12	< 0.001	107.87	588.71	< 0.001
s(FishID, Age)	94.36	42.22	< 0.001	85.93	35.62	< 0.001	97.36	291.04	< 0.001
s(Season x Site)	54.34	19.41	< 0.001	62.05	57.72	< 0.001	57.20	67.73	< 0.001

3.2 Covariation in trace element incorporation

Covariation between elements during otolith formation was evident both within and among individuals, albeit with greater uncertainty at the among-individuals level, where several credible intervals overlapped zero (Fig. 5, Table A2).

Within individuals, most element pairs showed positive associations, meaning that short-term fluctuations in one element tended to be accompanied by concurrent changes in others during otolith formation (Fig. 5a, Table A2). The strongest association at this level occurred between Ba and Sr, while moderate positive associations were also evident for Mg–Mn and P–Sr. Weaker positive associations occurred for P with Ba, Mg, and B, and for B with Mg and Sr. Sr showed negative associations with Mg and Mn.

Among individuals, the direction of correlations was broadly similar to the within-individual pattern. Sr–Ba remained the strongest positive association, showing that individuals with elevated Sr overall also tend to exhibit higher Ba (Fig. 5b, Table A2). Correlations among Mg–Mn, Mg–B and P–Ba were also positive. B and Ba were positively associated with each other and with Mn.

https://doi.org/10.5194/egusphere-2026-4521
Preprint. Discussion started: 7 August 2026

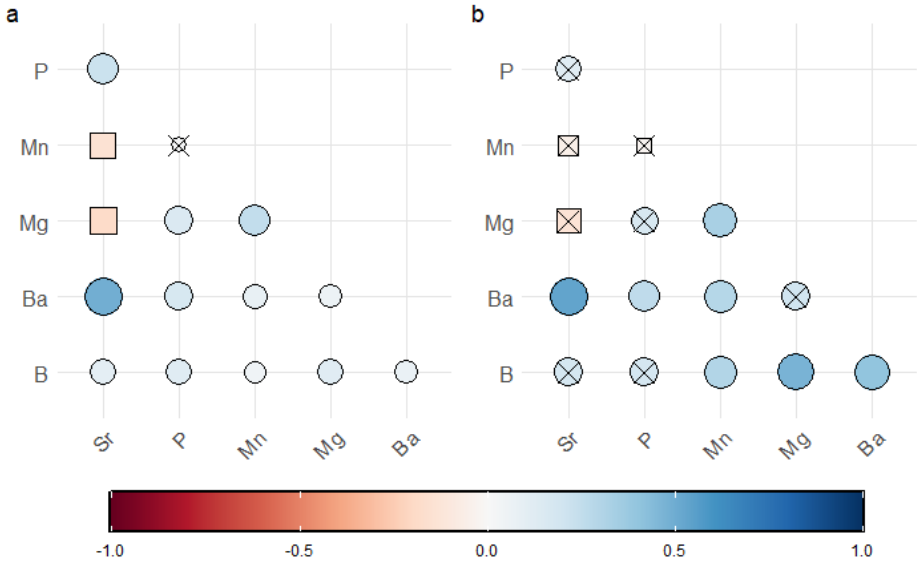

Figure 5 Within (a) and among (b) individual correlations of element pairs measured from otoliths of *B. glaciale*. Negative and positive correlations are indicated by red squares and blue circles respectively. Shading and size of the symbols reflect the magnitude of the effect. Correlations whose 95% credible intervals overlap zero are crossed out.

4 Discussion

This study provides the first age-resolved description of otolith trace-element incorporation in the glacier lanternfish *Benthosema glaciale*. Element:Ca ratios changed strongly with age, with several shifts occurring around ages 2–3, close to the reported onset of sexual maturation in this region (Gjøsæter, 1981). The clearest ecological signal came from Sr:Ca and Ba:Ca: their trajectories are consistent with a shift from surface-influenced waters in early life toward deeper, stratified water masses in older fish. Mg:Ca and Mn:Ca were highest early in life and then declined, consistent with reduced growth and metabolic activity. P:Ca and B:Ca showed additional age- and site-related structure, but their interpretation was less direct. Spatial structure was strongest between the coastal site and the fjords, and individual fish differed persistently in both overall element levels and age trajectories, showing that population-level chemical patterns are built from heterogeneous individual histories.

4.1 Ontogenetic deepening and water-mass exposure encoded by Sr and Ba

Sr and Ba are among the most widely applied tracers in otolith chemistry due to their established links with environmental concentrations and physical gradients in marine systems (Bath et al., 2000). Sr generally tracks water-mass structure and salinity variations (Walther and Limburg, 2012). At the same time, Sr uptake is known to be modulated by physiological factors including growth rate, with faster-growing individuals typically showing lower Sr (Grammer et al., 2017; Sturrock et

https://doi.org/10.5194/egusphere-2026-4521
Preprint. Discussion started: 7 August 2026

al., 2015). Ba is often linked to productivity, freshwater influence and regeneration at depth, and can vary strongly across coastal and fjord water masses (Guay and Kenison Falkner, 1997; Hüssy et al., 2020).

In *B. glaciale*, both otolith Sr and Ba displayed trajectories consistent with ontogenetic shifts across depth-structured water masses. Sr:Ca tended to increase throughout life, whereas Ba:Ca declined through juvenile stages and increased again in adults. These patterns match independent observations that *B. glaciale* occupies deeper waters after maturation (Dypvik et al., 2012b). They also match the vertical structure of west-Norwegian fjords, where surface-influenced layers, intermediate waters and deeper basin waters differ in salinity, oxygen and trace-element availability (Fig. A1, Fig. A2).

The juvenile Sr pattern was less straightforward than the adult pattern. Sr:Ca showed a small peak early in life, followed by a dip around ages 1–2. In early life, a mixture of rapid growth, variable depth use, and seasonal exposure to surface-influenced layers is likely to modulate or obscure environmentally driven signals, consistent with growth-related dilution effects and temperature sensitivity of Sr incorporation (Stanley et al., 2015). As individuals mature and depth use stabilises below productive surface layers, Sr:Ca increases more consistently, supporting longer exposure to deeper, more marine-influenced water masses. Future studies could test whether the early Sr:Ca peak and subsequent decline provide a chemical indicator of juvenile depth-use transitions, and whether the timing or strength of this feature varies with individual growth history or environmental conditions.

Consistent with physiological modulation of Sr:Ca, within-individual element correlations revealed a moderate but significant negative association between Sr:Ca and the metabolic tracers Mg:Ca and Mn:Ca. Since elevated Mg and Mn are typically linked to periods of higher metabolic activity and faster growth (Sturrock et al., 2015), this pattern supports growth-mediated dilution of Sr during phases of rapid otolith accretion and reinforces the interpretation that Sr incorporation reflects both environmental exposure and intrinsic physiological regulation.

Within this framework, the persistent sub-annual oscillations apparent in Sr:Ca trajectories—broadly corresponding to alternating growth phases—may reflect further interactions between seasonally-structured behaviour and physiological modulation. Seasonal changes in depth use and diel vertical migration direction have been documented for adult *B. glaciale* in the region (Dypvik et al., 2012b), with such behaviour likely to affect population-level environmental exposure despite the low seasonality in temperature and salinity and at depth.

Spatially, Sr:Ca was lower at the coastal site and generally higher in fjord fish. Although coastal waters can reach high salinity at depth, stronger mixing at the coast likely reduces persistent exposure to Sr-rich water masses. In contrast, fjord sites showed broadly similar Sr:Ca levels, reflecting more persistent stratification and the consequent accumulation of water-mass signals over time (Stigebrandt, 2012). Among fjords, minor differences in adult Sr trajectories may reflect reduced or less effective renewal of deep waters due to distance from the coast or shallow sill depths. However, these effects are minor relative to the dominant coast–fjord contrast.

Notably, the Sr:Ca trajectory in *B. glaciale* differs from the only other age-resolved myctophid otolith chemistry study currently available. In *Diaphus thiollierei* from the Arabian Sea, otolith Sr declines rapidly during early life and then stabilises, interpreted as movement from high-salinity surface waters into more homogeneous deeper layers (Wu et al.,

https://doi.org/10.5194/egusphere-2026-4521
Preprint. Discussion started: 7 August 2026

2024). The opposite tendency in *B. glaciale* after age 2 is more likely linked to hydrographic setting than to species-specific Sr uptake. The Arabian Sea is characterised by evaporation-driven high surface salinities, whereas the west-Norwegian coast is highly freshwater-influenced due to riverine input and precipitation. In our sites, salinity approaches marine values below the halocline and varies little at depth (Fig. A2), so Sr:Ca is better interpreted as a record of time-integrated exposure to distinct water masses than as movement along a simple depth–salinity gradient.

Ba:Ca adds ecological context because its water-column behaviour differs from that of Sr. In open-ocean settings, Ba is often low in productive surface waters due to adsorption onto biogenic particles and barite formation and higher at depth as sinking particles are remineralised (Hsieh and Henderson, 2017). In estuarine and fjord systems, river input and biological processing can add Ba to surface-influenced waters, while deeper waters can become enriched through regeneration (Guay and Kenison Falkner, 1997). The water-column Ba profiles from our fjord sites (Fig. A1) show this layered structure, with lower Ba at intermediate depths (~150–200 m) and higher values near the surface and in deeper water. Against this background, juvenile *B. glaciale* are likely exposed primarily to Ba-enriched surface waters, with maturing individuals increasingly occupying Ba-depleted layers and adults residing predominantly in Ba-enriched deep-basin waters—patterns consistent with the U-shaped Ba:Ca trajectory recorded in otoliths.

SOG shows higher Ba:Ca early in life and again in adults than the other sites. SOG has the shallowest sill and the highest watershed-to-fjord-surface ratio among the sampled basins (Saltalamacchia et al., 2026). Unsurprisingly, our CTD profiles show lower salinity there than at other sites (Fig. A2). Otolith Ba:Ca often increases under river-influenced, lower-salinity conditions in estuarine settings (Dorval et al., 2007; Elsdon and Gillanders, 2005). While we cannot infer this mechanism directly because water-column Ba data are unavailable for SOG, the overall otolith pattern is consistent with a stronger surface-water influence at that site.

The multivariate results support the interpretation of Sr and Ba as linked water-mass tracers. Sr:Ca and Ba:Ca were strongly and positively correlated both within and among adult fish after accounting for age, site, and individual trajectories. Since Sr^{2+} and Ba^{2+} have similar ionic radii and chemical behaviour and can substitute for Ca^{2+} within the aragonitic otolith lattice (Bath et al., 2000), shared environmental availability can be efficiently recorded as covariation when water-mass exposure covaries. Such coupling is expected if both elements respond to shared exposure to depth-structured water masses, rather than only reflecting parallel age trends.

4.2 B as a tentative carbonate-system signal?

B:Ca showed weaker age structure than the other elements, with site separation appearing mainly in older fish. The mechanisms controlling B incorporation in fish otoliths remain poorly resolved (Heimbrand and Limburg, 2025). Whereas dissolved B correlates with salinity (Lee et al., 2010), its incorporation into marine carbonates is linked to carbonate chemistry because the availability of borate (the species preferentially incorporated into calcium carbonates) increases with pH (Hemming and Hanson, 1992). In fish otoliths, recent studies on cod suggest that B:Ca may respond not only to pH and

https://doi.org/10.5194/egusphere-2026-4521
Preprint. Discussion started: 7 August 2026

oxygen conditions, but also to physiological state and possibly other, yet unknown, environmental sources (Heimbrand and Limburg, 2025; Limburg et al., 2023).

In our data, B:Ca was relatively low or flat at the coastal site and tended to be higher in older fish from some fjords. This weak pattern broadly follows the hydrographic gradient from more open systems (COA and FEN) to basins situated behind shallower sills or further inland (MAS, OST, SOG and SØR), and is compatible with long-term exposure to more enclosed basin waters where residence time, ventilation and organic matter remineralisation can affect carbonate chemistry (Asplin et al., 1999; Atamanchuk et al., 2015; Hare et al., 2020; Omar et al., 2016). At the same time, B:Ca was positively associated with Mg:Ca among individuals, suggesting that physiological state or biomineralisation may also influence the signal. Because we lack carbonate-system measurements at these sites, B:Ca cannot be directly linked to pH or buffering capacity here. These patterns should therefore be seen as exploratory signals that may reflect environmental exposure, physiology, or both.

4.3 Mg, Mn, P as physiological indicators

Mg:Ca and Mn:Ca both declined through life, consistent with expectations from growth- and metabolism-linked tracers (Hüssy et al., 2020; Limburg et al., 2015, 2018). The positive Mg–Mn association at both within- and among-individual levels further supports a shared physiological component in their incorporation.

Mg:Ca declined steadily with age in the fjords, whereas the coastal trajectory showed a clear peak around age 1 before declining. This peak may reflect stronger juvenile growth conditions at the coast, consistent with larger otolith increments at juvenile ages in COA (Fig. A3). After early life, Mg:Ca trajectories became more similar among sites, possibly linked to a shift from site-specific juvenile growth conditions to a more similar adult physiological state after maturation.

Mn:Ca closely followed Mg:Ca, with both elements showing high values early in life and declining toward adulthood. This shared pattern, together with the positive Mg–Mn associations at both within- and among-individual levels, points to a strong physiological component in Mn incorporation. Mg and Mn are both influenced by growth, metabolism and biomineralisation processes, so part of the Mn decline likely reflects the same ontogenetic shift that drives the Mg pattern (Hüssy et al., 2020; Limburg et al., 2015, 2018). However, Mn may also record environmental components. In coastal and shelf waters, dissolved Mn can be elevated by terrestrial input, sediment exchange and regeneration under reducing conditions, while concentrations are often low in well-oxygenated deep waters (Brinkmann et al., 2023; Hamilton-Taylor and Price, 1983). The decline in Mn:Ca with age is therefore also consistent with fish moving away from shallow or more coastally influenced water layers as they mature.

The redox signal was weaker than expected. Mn availability can increase under low-oxygen conditions when sediment Mn is released into overlying water (Limburg et al., 2015), and increased Mn^{2+} has been observed near the seafloor in Masfjord after a prolonged hypoxic event (Ferraro et al., 2025). In our otoliths, however, although some slight differences (especially at ages 4-5) might be observed between the well-ventilated COA/FEN and the inner fjords, adult Mn:Ca did not show strong

https://doi.org/10.5194/egusphere-2026-4521
Preprint. Discussion started: 7 August 2026

enrichment in fjords with lower deep-water oxygen (MAS, SOG, SØR; Fig. A2, Fig. A4). Under the conditions sampled here, physiological control and declining exposure to shallow/coastal Mn sources appear to dominate the Mn:Ca trajectory. Importantly, otolith Mn:Ca is not a deterministic marker of hypoxia in wild fish, and individuals from hypoxic and normoxic sites can show overlapping values (Limburg et al., 2015). Low oxygen alone may also be insufficient unless it produces enough dissolved Mn in the water column occupied by fish (Mohan et al., 2022), which may require more strongly reducing conditions than many fish regularly occupy (Limburg et al., 2015). Because oxygen loss in our study system was generally moderate (Fig. A2), and sampling targeted mid-water habitats, demersal and benthic fish living close to Mn-enriched bottom waters could still record a stronger redox-driven signal than resolved here.

Otolith P:Ca is generally treated as a physiology- or biomineralisation-linked signal, although the mechanisms controlling P incorporation remain poorly resolved (Hüssy et al., 2020) and clear interannual patterns between opaque and translucent zones were not observed in our data. In *B. glaciale*, P:Ca was relatively flat during juvenile life and increased from around age 2, close to the age at which individuals begin to mature in western Norway (Gjøsæter, 1981). This pattern fits a maturation-related change in otolith biomineralisation or energy allocation. In marine teleosts, elevated P:Ca has been associated with periods of active growth and ontogenetic transitions (Borelli et al., 2003). The flatter, lower adult P:Ca trajectory at COA, despite larger body size, indicates that P:Ca does not simply scale with somatic growth. One possible explanation is that coastal and fjord fish differ in adult energy allocation. Spatial differences in reproductive investment have been reported in the co-occurring mesopelagic fish *Maurolicus muelleri*, with lower gonadosomatic index at the coast than in a fjord site (Salvanes and Stockley, 1996), and broader fjord–ocean differences in gonad weight and condition (Kristoffersen and Salvanes, 1998).

4.4 Persistent individual chemical signatures and ecological heterogeneity

Persistent individual differences were a major feature of *B. glaciale* otolith chemistry. Individuals differed in both overall element levels and age trajectories, indicating substantial within-site heterogeneity which may reflect differences in behaviour, physiology, or time-integrated exposure histories within the same site. In this study, the pronounced heterogeneity may be linked to the environmental context experienced by mesopelagic fish in a fjord–shelf system characterised by vertical gradients and site contrasts. Acoustic studies in fjord and coastal systems show that mesopelagic organisms can vary in diel vertical migration behaviour, including partial and asynchronous migration patterns (Dypvik et al., 2012b; Kaartvedt et al., 2008; Vestheim et al., 2014), providing a plausible behavioural context for the individual chemical signatures observed here.

By explicitly resolving age-dependent and individual-level structure, this study also clarifies that the previously reported chemical differentiation among sites (Saltalamacchia et al., 2026) is not uniformly shared by all fish, but emerges as a population-level average built from heterogeneous individual histories. This is important when using otolith chemistry to infer spatial structure in species with ontogenetic depth shifts or for which sampling depth, gear selectivity, or seasonal timing influence the age structure of catches.

https://doi.org/10.5194/egusphere-2026-4521
Preprint. Discussion started: 7 August 2026

Our results also highlight that rigid classification of otolith elements as strictly "environmentally driven" or "physiologically regulated" may be overly simplistic. The strength and structure of elemental signals depend not only on elemental properties but also on ecological context, life-history strategy, and habitat structure. In mesopelagic fishes such as *B. glaciale*, progressive ontogenetic deepening and seasonally modulated vertical behaviour within strongly stratified systems can amplify environmentally structured signals that may be weak or obscured in other systems. In this sense, fjords function as natural experiments in vertical ecology, allowing otolith chemistry to assess habitat use at biologically relevant scales.

4.5 Limitations and future work

A small proportion of measurements (< 4% across all transects, and < 2% for most elements) required interpolation because they were below detection limits or identified as isolated analytical artefacts. This approach was considered conservative and unlikely to bias the age-structured and spatial patterns reported here.

Assigning continuous ages within translucent and opaque increments required assumptions about seasonal deposition. This approach allowed fine-scale ontogenetic comparisons, but small site- or year-specific differences in deposition timing may affect short-term patterns, especially in early life. These uncertainties are unlikely to alter the main later-life trajectories or the dominant coast–fjord contrasts. Minor site-specific differences in otolith deposition timing, particularly at the coastal site, are likewise unlikely to strongly influence the results, given the consistent microchemical separation observed between coastal and fjord population components (Saltalamacchia et al., 2026).

Several avenues remain for strengthening inference from otolith chemistry in mesopelagic fishes. Targeted sampling of otolith edge composition across multiple seasons and age classes would improve resolution of sub-annual variability, particularly in early life stages. In parallel, concurrent time-series measurements of water chemistry would allow more explicit environmental matching and refine the interpretation of elemental incorporation. Although experimental validation remains challenging for mesopelagic species, comparative studies across systems with contrasting hydrography offer a feasible path toward constraining mechanistic understanding.

5 Conclusions

This study shows that otolith chemistry provides a time-integrated record of ontogenetic habitat use in *Benthosema glaciale* within a vertically structured environment, complementing snapshot information from trawl surveys or acoustic observations. By resolving element-specific chemical trajectories, we integrate previous evidence that the species undergoes progressive ontogenetic deepening accompanied by increasing spatial residency within fjord basins.

The ability retrospectively to infer depth-structured habitat use across ontogeny is particularly valuable in data-poor mesopelagic systems, where direct individual tracking and population monitoring remain impractical. By linking element-specific trajectories to known depth distributions and water-mass structure, otolith chemistry offers a practical framework for matching life-history processes and water-mass exposure over time, with clear relevance for understanding mesopelagic

https://doi.org/10.5194/egusphere-2026-4521
Preprint. Discussion started: 7 August 2026

ecosystem function, connectivity patterns, stage-specific vulnerability to commercial exploitation, and potential responses to ongoing environmental change.

Appendix A

Table A1 Candidate GAMM formulations used to model element-specific otolith element:calcium (E:Ca) trajectories. Models $m1_a$–$m1_b$ establish shared ontogenetic and individual-level structure; models $m2_a$–$m2_e$ compare alternative representations of site-level differences and site-specific age trajectories; models m3a–m3b add temporal growth-season structure to the best-supported spatial formulation. η represents the expected value of the response variable under a log-link. Fixed effects: β_0 represents the global intercept. f(age) a shared thin-plate smooth function of age. g_s(age) and f_s(age) denote site-specific age smooths using factor-smooths (different trajectories, same complexity) and thin-plate splines (different trajectories, different complexity), respectively; site is a categorical fixed effect describing sampling site identity. Random effects: b_i and b_i(age) are individual-level random intercepts and age slopes capturing among-fish differences in overall E:Ca and age trajectories. b_t is a random intercept for the sequential translucent–opaque depositions across the time span of all sampled increments (2013-2021). b_{ts} is a nested season × site random intercept. In $m3_a$ and $m3_b$, "[.]" denotes the best formulation (based on AIC) among the different spatial formulations ($m2_a$-$m2_e$). Bold font identifies model formulations selected for at least one element, and used for interpretation

Model	Formulation	Model rationale
$m1_a$	$\eta = \beta_0 + f(\text{age}) + b_i$	Minimal shared-age model. All sites share one population-level age trajectory(f(age)), while individuals differ in overall E:Ca across life (b_i).
$m1_b$	$\eta = \beta_0 + f(\text{age}) + b_i + b_i(\text{age})$	Individuals differ in both overall elemental concentration and how the E:Ca trajectory changes with age (b_i(age)).
$m2_a$	$\eta = \beta_0 + f(\text{age}) + \text{site} + b_i + b_i(\text{age})$	In addition to $m1_b$, sampling sites also differ in average elemental concentrations (site).
$m2_b$	$\eta = \beta_0 + f(\text{age}) + g_s(\text{age}) + b_i + b_i(\text{age})$	In addition to $m1_b$, the common ontogenetic trend is also modulated by site-specific deviations of identical complexity (factor-smooth formulation; g_s(age)).
$m2_c$	$\eta = \beta_0 + g_s(\text{age}) + b_i + b_i(\text{age})$	No common age trend — each site has its own age-related chemical trajectory, with all site trajectories fitted under the same smoothness constraint.
$m2_d$	$\eta = \beta_0 + f(\text{age}) + \text{site} + f_s(\text{age}) + b_i + b_i(\text{age})$	The common ontogenetic trend is modulated by site-specific deviations, with site trajectories allowed to differ in complexity (thin-plate formulation; f_s(age)).
$m2_e$	$\eta = \beta_0 + \text{site} + f_s(\text{age}) + b_i + b_i(\text{age})$	No common age trend — each site has its own age-related chemical trajectory, with site trajectories allowed to differ in complexity.
$m3_a$	$\eta = [.] + b_t$	Allows the recurring translucent–opaque deposition phases across all sampled years to shift overall elemental levels, capturing consistent chemical differences between growth phases through time (b_t).
$m3_b$	$\eta = [.] + b_{ts}$	Allows season × site deviations, enabling otoliths from different sites and growth seasons to differ in their overall chemical signal (b_{ts}).

https://doi.org/10.5194/egusphere-2026-4521
Preprint. Discussion started: 7 August 2026

Table A2 Within- and among-individual correlations between otolith trace element ratios in *Benthosema glaciale* estimated from multivariate mixed-effects models (Hadfield, 2010). Posterior means and 95% credible intervals (CrI) are shown after accounting for age, site, and individual effects. Positive or negative relationships indicate credible intervals excluding zero.

Element pair	Correlation type	Posterior mean	Lower 95% CrI	Upper 95% CrI	Relationship
B11 - Ba138	Within	0.066	0.030	0.101	Positive
B11 - Ba138	Among	0.398	0.193	0.576	Positive
B11 - Mg25	Within	0.115	0.080	0.150	Positive
B11 - Mg25	Among	0.465	0.269	0.638	Positive
B11 - Mn55	Within	0.036	0.000	0.071	Positive
B11 - Mn55	Among	0.299	0.081	0.499	Positive
B11 - P31	Within	0.125	0.090	0.160	Positive
B11 - P31	Among	0.183	-0.034	0.382	Null
B11 - Sr88	Within	0.100	0.066	0.136	Positive
B11 - Sr88	Among	0.185	-0.045	0.400	Null
Ba138 - Mg25	Within	0.064	0.028	0.100	Positive
Ba138 - Mg25	Among	0.199	-0.021	0.408	Null
Ba138 - Mn55	Within	0.082	0.047	0.117	Positive
Ba138 - Mn55	Among	0.293	0.083	0.482	Positive
Ba138 - P31	Within	0.168	0.133	0.201	Positive
Ba138 - P31	Among	0.260	0.061	0.443	Positive
Ba138 - Sr88	Within	0.489	0.461	0.516	Positive
Ba138 - Sr88	Among	0.530	0.356	0.677	Positive
Mg25 - Mn55	Within	0.253	0.221	0.287	Positive
Mg25 - Mn55	Among	0.330	0.117	0.515	Positive
Mg25 - P31	Within	0.150	0.115	0.184	Positive
Mg25 - P31	Among	0.173	-0.039	0.375	Null
Mg25 - Sr88	Within	-0.194	-0.228	-0.160	Negative
Mg25 - Sr88	Among	-0.144	-0.361	0.082	Null
Mn55 - P31	Within	0.009	-0.026	0.045	Null
Mn55 - P31	Among	-0.031	-0.235	0.175	Null
Mn55 - Sr88	Within	-0.146	-0.180	-0.110	Negative

https://doi.org/10.5194/egusphere-2026-4521
Preprint. Discussion started: 7 August 2026

Element pair	Correlation type	Posterior mean	Lower 95% CrI	Upper 95% CrI	Relationship
Mn55 - Sr88	Among	-0.056	-0.277	0.164	Null
P31 - Sr88	Within	0.217	0.182	0.250	Positive
P31 - Sr88	Among	0.117	-0.099	0.320	Null

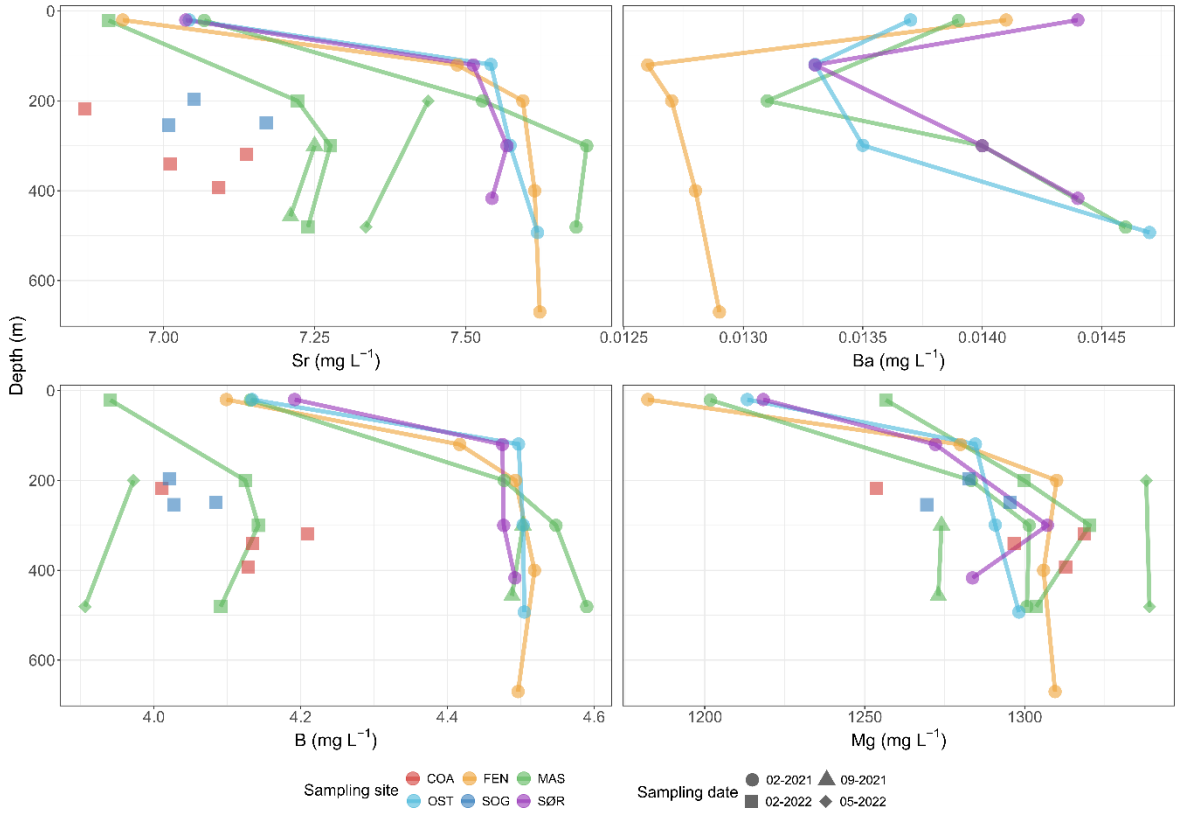

585 **Figure A1 Water chemistry profiles for Sr, Ba, B and Mg collected over the six sampling sites along the Norwegian west coast. Measurements connected by lines were collected within the same CTD cast. Site abbreviations: COA (Coastal), FEN (Fensfjord), MAS (Masfjord), OST (Osterfjord), SOG (Sogndalsfjord), SØR (Sørfjord). Additional information about samples taken during the IMR CoastRisk cruise (02-2022) can be found in the technical report (Søvik et al., 2023).**

https://doi.org/10.5194/egusphere-2026-4521
Preprint. Discussion started: 7 August 2026

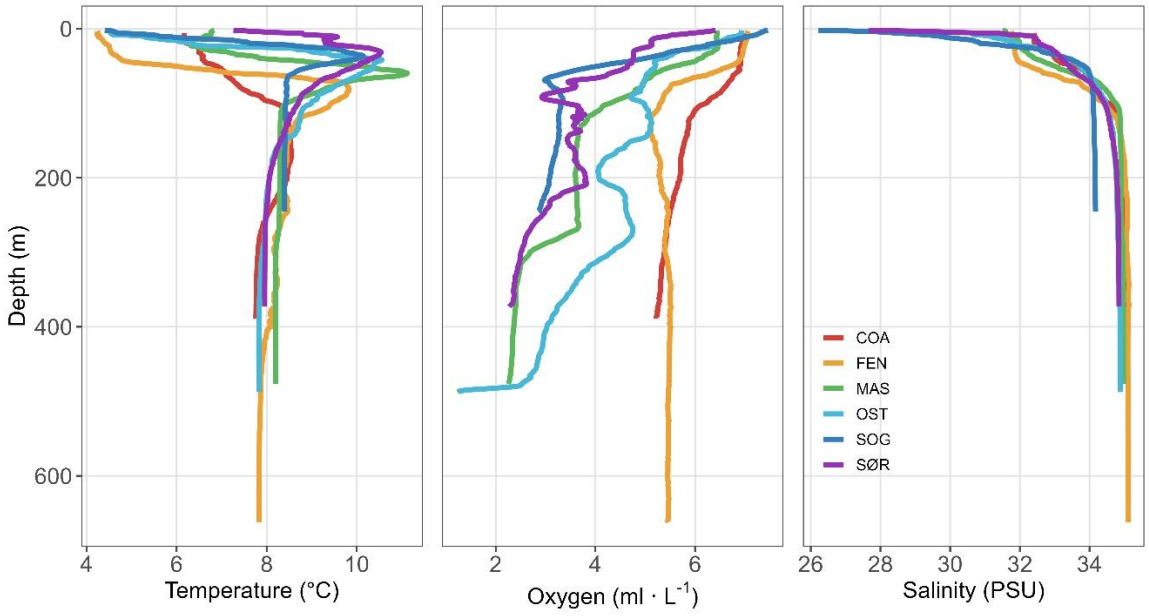

590 **Figure A2 Temperature, oxygen and salinity profiles collected by Seabird CTD at the six sampling sites in February 2021 (FEN, MAS, OST, SØR) and February 2022 (COA, SOG). From: Saltalamacchia et al. (2026).**

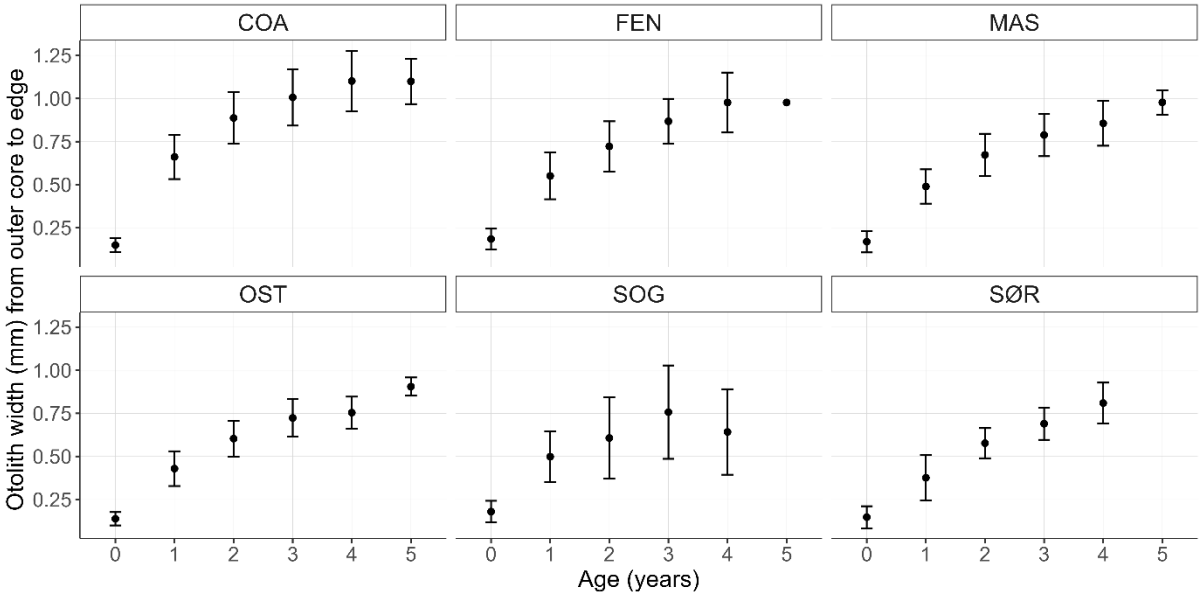

Figure A3 Mean cumulative otolith distance at age in *B. glaciale*, measured from the outer edge of the core along the dorsal side of ablated otolith sections. Points show site-specific means at each age landmark, and error bars show ± standard deviation.
595 **Landmark 0 represents the first measured position outside the core, and subsequent landmarks correspond to successive annual age boundaries.**

https://doi.org/10.5194/egusphere-2026-4521
Preprint. Discussion started: 7 August 2026

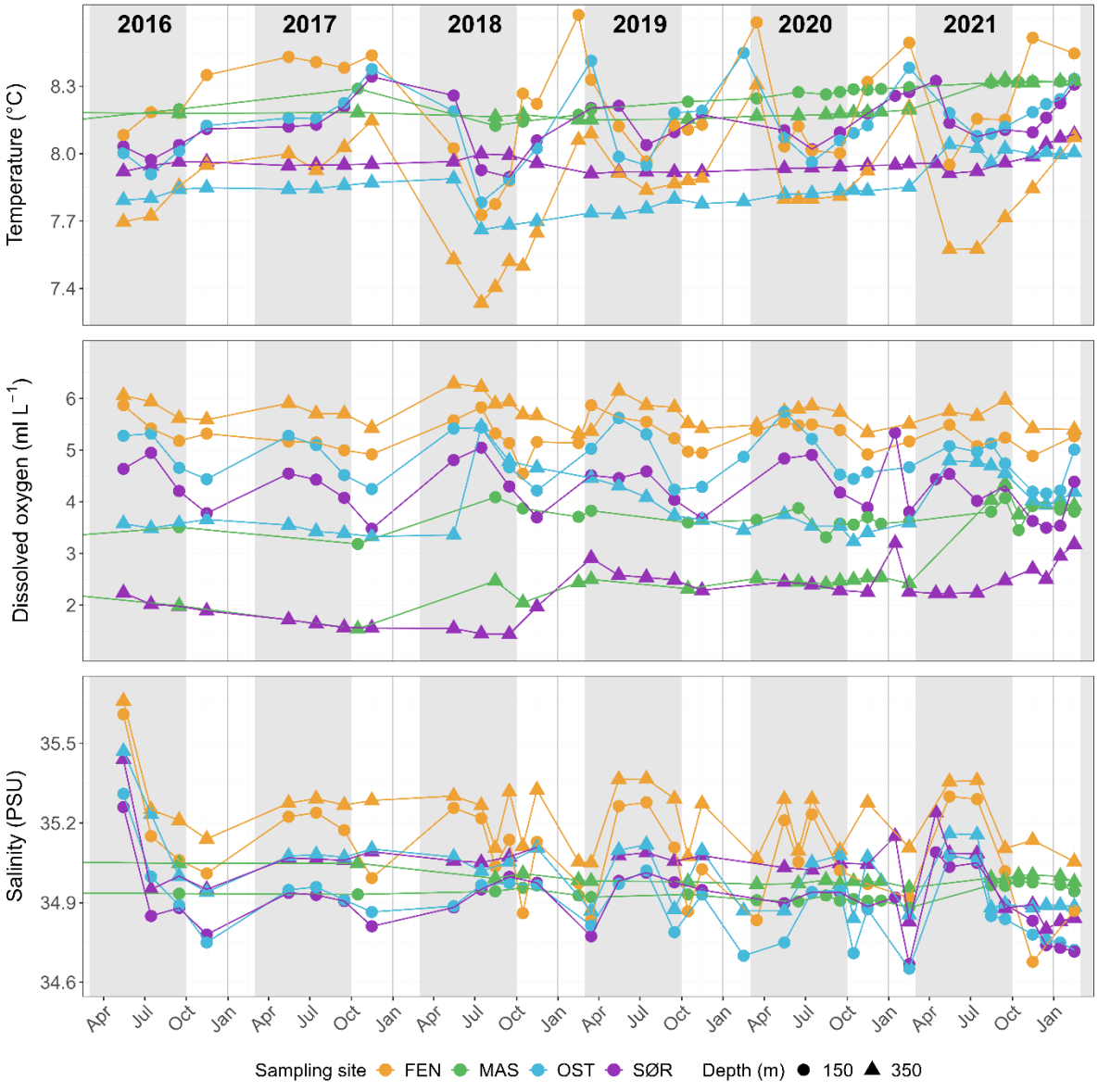

Figure A4 Time series of temperature, oxygen and salinity measured at 150 (circles) and 350 m depth (triangles) in FEN, MAS, OST and SØR from 2016 to 2021. Background shading follows the seasonality assigned to otolith increments based on Gjøsæter (1973): March-September, translucent (lighter background); October-February, opaque (darker). Hydrographic data comes from surveys conducted by the University of Bergen (UiB), or collected by the Institute of Marine Research (IMR) and Blue Planet AS for the Norwegian Research Centre (NORCE). Hydrographic data originating from UiB are available through the Norwegian Marine Data Centre (https://nmdc.no/). Environmental monitoring datasets collected for NORCE are available on VannMiljø (https://vannmiljo.miljodirektoratet.no/).

https://doi.org/10.5194/egusphere-2026-4521
Preprint. Discussion started: 7 August 2026

Code and data availability

The otolith microchemical data used in this study and code to reproduce the main analyses are available on Zenodo: https://doi.org/10.5281/zenodo.21508611. Figures A2 and A4 use hydrographic data from surveys conducted by the University of Bergen (UiB) (Fig. A2) or collected by the Institute of Marine Research (IMR) and Blue Planet AS for the Norwegian Research Centre (NORCE) (Fig. A2, Fig. A4). Hydrographic data from UiB were downloaded from the Norwegian Marine Data Centre (https://nmdc.no). The environmental monitoring data collected for NORCE are available on VannMiljø (https://vannmiljo.miljodirektoratet.no).

Author contributions

FS and NDG designed the experiment, collected the samples, prepared and processed the otoliths using the LA-ICP MS instrumentation in KL's lab, and collected image data. FS performed data cleaning and processing, conducted the formal analysis and wrote the main text. KL contributed to conceptualisation, provided the instrumentation and guidance for collecting trace-element concentrations, and assisted with the formulation of hypotheses and the interpretation/discussion of the results. AF and AGVS supervised the project and assisted with the interpretation of results. AGVS was responsible for project administration and funding acquisition. All authors reviewed the manuscript.

Competing interests

The authors declare that they have no conflict of interest.

Acknowledgements

We thank Heikki Savolainen, Frank Midtøy and Julie Skadal (University of Bergen), as well as the crews of the research vessels *G.O. Sars*, *Kristine Bonnevie* and *Dr. Fridtjof Nansen* (Institute of Marine Research) for their essential role in collecting the material analysed in this study. We are also grateful to Debra Driscoll (ICP laboratory manager at the Analytical and Technical Services Group, SUNY ESF) for her tireless help to ensure successful data collection, including working late into the night with us; Clement Z. W. Ng (Nanyang Technological University) for sharing his R code; Blue Planet AS for granting access to their fjord hydrographic data; Bence Paul and Joe Petrus (Elemental Scientific Lasers) for providing a free Iolite student license and user support.

https://doi.org/10.5194/egusphere-2026-4521
Preprint. Discussion started: 7 August 2026

Financial support

This work was funded by the Research Council of Norway through the HypOnFjordFish project (UiB; project number 301077). Part of the otolith material was collected within the CoastRisk project (IMR), funded by the Research Council of Norway (project number 299554).

References

Aksnes, D. L., Aure, J., Johansen, P. O., Johnsen, G. H., and Salvanes, A. G. V.: Multi-decadal warming of Atlantic water and associated decline of dissolved oxygen in a deep fjord, Estuar. Coast. Shelf Sci., 228, 106392, https://doi.org/10.1016/J.ECSS.2019.106392, 2019.

Asplin, L., Salvanes, A. G. V., and Kristoffersen, J. B.: Nonlocal wind-driven fjord–coast advection and its potential effect on plankton and fish recruitment, Fish. Oceanogr., 8, 255–263, https://doi.org/10.1046/j.1365-2419.1999.00109.x, 1999.

Atamanchuk, D., Kononets, M., Thomas, P. J., Hovdenes, J., Tengberg, A., and Hall, P. O. J.: Continuous long-term observations of the carbonate system dynamics in the water column of a temperate fjord, J. Mar. Syst., 148, 272–284, https://doi.org/10.1016/j.jmarsys.2015.03.002, 2015.

Bath, G. E., Thorrold, S. R., Jones, C. M., Campana, S. E., McLaren, J. W., and Lam, J. W. H.: Strontium and barium uptake in aragonitic otoliths of marine fish, Geochim. Cosmochim. Acta, 64, 1705–1714, https://doi.org/10.1016/S0016-7037(99)00419-6, 2000.

Borelli, G., Mayer-Gostan, N., Merle, P., De Pontual, H., Boeuf, G., Allemand, D., and Payan, P.: Composition of biomineral organic matrices with special emphasis on turbot (Psetta maxima) otolith and endolymph, Calcif. Tissue Int., 72, 717–725, 2003.

Brinkmann, I., Barras, C., Jilbert, T., Næraa, T., Paul, K. M., Schweizer, M., and Filipsson, H. L.: Drought recorded by Ba/Ca in coastal benthic foraminifera, Biogeosciences, 19, 2523–2535, https://doi.org/10.5194/bg-19-2523-2022, 2022.

Brinkmann, I., Barras, C., Jilbert, T., Paul, K. M., Somogyi, A., Ni, S., Schweizer, M., Bernhard, J. M., and Filipsson, H. L.: Benthic Foraminiferal Mn/Ca as Low-Oxygen Proxy in Fjord Sediments, Glob. Biogeochem. Cycles, 37, e2023GB007690, https://doi.org/10.1029/2023GB007690, 2023.

Campana, S. E.: Chemistry and composition of fish otoliths: pathways, mechanisms and applications, Mar. Ecol. Prog. Ser., 188, 263–297, 1999.

Catul, V., Gauns, M., and Karuppasamy, P. K.: A review on mesopelagic fishes belonging to family Myctophidae, Rev. Fish Biol. Fish., 21, 339–354, https://doi.org/10.1007/S11160-010-9176-4, 2011.

Cavole, L. M., Limburg, K. E., Gallo, N. D., Vea Salvanes, A. G., Ramírez-Valdez, A., Levin, L. A., Oropeza, O. A., Hertwig, A., Liu, M.-C., and McKeegan, K. D.: Otoliths of marine fishes record evidence of low oxygen, temperature and pH conditions of deep Oxygen Minimum Zones, Deep Sea Res. Part Oceanogr. Res. Pap., 191, 103941, https://doi.org/10.1016/j.dsr.2022.103941, 2023.

Clarke, L. B. and Sloss, L. L.: Trace elements, EA Coal Res., IEACR/49, 1992.

https://doi.org/10.5194/egusphere-2026-4521
Preprint. Discussion started: 7 August 2026

Degens, E. T., Deuser, W. G., and Haedrich, R. L.: Molecular structure and composition of fish otoliths, Mar. Biol., 2, 105–113, https://doi.org/10.1007/BF00347005, 1969.

Dorval, E., Jones, C., Hannigan, R., and Montfrans, J.: Relating otolith chemistry to surface water chemistry in a coastal plain estuary, Can. J. Fish. Aquat. Sci., 64, 411–424, https://doi.org/10.1139/F07-015, 2007.

Dypvik, E., Klevjer, T. A., and Kaartvedt, S.: Inverse vertical migration and feeding in glacier lanternfish (Benthosema glaciale), Mar. Biol., 159, 443–453, https://doi.org/10.1007/s00227-011-1822-4, 2012a.

Dypvik, E., Røstad, A., and Kaartvedt, S.: Seasonal variations in vertical migration of glacier lanternfish, Benthosema glaciale, Mar. Biol., 159, 1673–1683, https://doi.org/10.1007/s00227-012-1953-2, 2012b.

Eduardo, L. N., Bertrand, A., Mincarone, M. M., Martins, J. R., Frédou, T., Assunção, R. V., Lima, R. S., Ménard, F., Le Loc'h, F., and Lucena-Frédou, F.: Distribution, vertical migration, and trophic ecology of lanternfishes (Myctophidae) in the Southwestern Tropical Atlantic, Prog. Oceanogr., 199, 102695, https://doi.org/10.1016/j.pocean.2021.102695, 2021.

Elsdon, T. S. and Gillanders, B. M.: Consistency of patterns between laboratory experiments and field collected fish in otolith chemistry: an example and applications for salinity reconstructions, Mar. Freshw. Res., 56, 609–617, https://doi.org/10.1071/MF04146, 2005.

Ferraro, M., Risebrobakken, B., Polovodova Asteman, I., Darelius, E., Tisserand, A., Gallo, N. D., and Salvanes, A. G. V.: The Present-Day Relation Between Observed Bottom Water Oxygenation and Marine Oxygen Proxies, Glob. Biogeochem. Cycles, 39, e2024GB008334, https://doi.org/10.1029/2024GB008334, 2025.

Gauthier, C., Fisher, J. A. D., Robert, D., and Sirois, P.: Otoliths as chemical archives through ontogeny reveal distinct migratory strategies of Atlantic halibut within the Gulf of St. Lawrence, ICES J. Mar. Sci., 81, 1221–1233, https://doi.org/10.1093/icesjms/fsae081, 2024.

Giske, J., Aksnes, D. L., Baliño, B. M., Kaartvedt, S., Lie, U., Nordeide, J. T., Salvanes, A. G. V., Wakili, S. M., and Aadnesen, A.: Vertical distribution and trophic interactions of zooplankton and fish in Masfjorden, Norway, SARSIA, 75, 65–81, https://doi.org/10.1080/00364827.1990.10413442, 1990.

Gjøsæter, J.: Age, Growth, Reproduction, and Feeding of Benthosema glaciale (Myctophidae) from Western Norway, Int. Counc. Explor. Sea Pelagic Fish North. Comm., C.M. 1970/, 1–13, 1970.

Gjøsæter, J.: Age, growth, and mortality of the myctophid fish, Benthosema glaciale (Reinhardt), from western Norway, Sarsia, 52, 1–14, 1973.

Gjøsæter, J.: Growth, production and reproduction of the myctophid fish Benthosema glaciale from western Norway and adjacent seas, FiskDir Skr Ser HavlJnders, 17, 79–108, 1981.

Gjøsaeter, J. and Kawaguchi, K.: A review of the world resources of mesopelagic fish, FAO Fish. Tech. Pap., 193, 123–134, 1980.

Grammer, G. L., Morrongiello, J. R., Izzo, C., Hawthorne, P. J., Middleton, J. F., and Gillanders, B. M.: Coupling biogeochemical tracers with fish growth reveals physiological and environmental controls on otolith chemistry, Ecol. Monogr., 87, 487–507, https://doi.org/10.1002/ecm.1264, 2017.

Guay, C. K. and Kenison Falkner, K.: Barium as a tracer of Arctic halocline and river waters, Deep Sea Res. Part II Top. Stud. Oceanogr., 44, 1543–1569, https://doi.org/10.1016/S0967-0645(97)00066-0, 1997.

https://doi.org/10.5194/egusphere-2026-4521
Preprint. Discussion started: 7 August 2026

Hadfield, J. D.: MCMC Methods for Multi-Response Generalized Linear Mixed Models: The MCMCglmm R Package, J. Stat. Softw., 33, 1–22, https://doi.org/10.18637/jss.v033.i02, 2010.

Halliday, R. G.: Growth and vertical distribution of the glacier lanternfish, Benthosema glaciale, in the northwestern Atlantic, J. Fish. Board Can., 27, 105–116, 1970.

Hamilton-Taylor, J. and Price, N. B.: The geochemistry of iron and manganese in the waters and sediments of Bolstadfjord, S.W. Norway, Estuar. Coast. Shelf Sci., 17, 1–19, https://doi.org/10.1016/0272-7714(83)90041-0, 1983.

Hare, A., Evans, W., Pocock, K., Weekes, C., and Gimenez, I.: Contrasting marine carbonate systems in two fjords in British Columbia, Canada: Seawater buffering capacity and the response to anthropogenic CO2 invasion, PLOS ONE, 15, e0238432, https://doi.org/10.1371/journal.pone.0238432, 2020.

Heimbrand, Y. and Limburg, K. E.: Elevated boron in cod otoliths from the low-salinity Åland Sea: A unique marker for a new population in the Baltic Sea?, Mar. Coast. Fish., 17, vtaf022, https://doi.org/10.1093/mcfafs/vtaf022, 2025.

Helle, H. B.: Summer Replacement of Deep Water in Byfjord, Western Norway: Mass Exchange Across the Sill Induced by Coastal Upwelling, Elsevier Oceanogr. Ser., 23, 441–464, https://doi.org/10.1016/S0422-9894(08)71293-5, 1978.

Hemming, N. G. and Hanson, G. N.: Boron isotopic composition and concentration in modern marine carbonates, Geochim. Cosmochim. Acta, 56:1, https://doi.org/10.1016/0016-7037(92)90151-8, 1992.

Hidalgo, M. and Browman, H. I.: Developing the knowledge base needed to sustainably manage mesopelagic resources, ICES J. Mar. Sci., 76, 609–615, https://doi.org/10.1093/ICESJMS/FSZ067, 2019.

Hjelstuen, B. O., Kjennbakken, H., Bleikli, V., Ersland, R. A., Kvilhaug, S., Euler, C., and Alvheim, S.: Fjord stratigraphy and processes – evidence from the NE Atlantic Fensfjorden system, J. Quat. Sci., 28, 421–432, https://doi.org/10.1002/jqs.2636, 2013.

Hsieh, Y.-T. and Henderson, G. M.: Barium stable isotopes in the global ocean: Tracer of Ba inputs and utilization, Earth Planet. Sci. Lett., 473, 269–278, https://doi.org/10.1016/j.epsl.2017.06.024, 2017.

Hüssy, K., Limburg, K. E., de Pontual, H., Thomas, O. R. B., Cook, P. K., Heimbrand, Y., Blass, M., and Sturrock, A. M.: Trace element patterns in otoliths: the role of biomineralization, Rev. Fish. Sci. Aquac., 1–33, 2020.

Hüssy, K., Albertsen, C. M., Hemmer-Hansen, J., Vinther, M., Serre, S. H., Thomsen, T. B., and Eero, M.: Where do you come from, where do you go: early life stage drift and migrations of cod inferred from otolith microchemistry and genetic population assignment, Can. J. Fish. Aquat. Sci., 79, 300–313, https://doi.org/10.1139/cjfas-2020-0409, 2022.

Kaartvedt, S., Aksnes, D. L., and Aadnesen, A.: Winter distribution of macroplankton and micronekton in Masfjorden, western Norway, Mar. Ecol. Prog. Ser., 45, 45–55, 1988.

Kaartvedt, S., Torgersen, T., Klevjer, T. A., Røstad, A., and Devine, J. A.: Behavior of individual mesopelagic fish in acoustic scattering layers of Norwegian fjords, Mar. Ecol. Prog. Ser., 360, 201–209, https://doi.org/10.3354/MEPS07364, 2008.

Knutsen, T., Strand, E., Klevjer, T. A., Salvanes, A. G. V., Broms, C., Sunde, S. M., Aksnes, D. L., García-Seoane, E., and Melle, W.: Feeding ecology of Benthosema glaciale across the North Atlantic, Front. Mar. Sci., 10, 1086607, https://doi.org/10.3389/fmars.2023.1086607, 2023.

https://doi.org/10.5194/egusphere-2026-4521
Preprint. Discussion started: 7 August 2026

Kristoffersen, J. B. and Salvanes, A. G. V.: Life history of Maurolicus muelleri in fjordic and oceanic environments, J. Fish Biol., 53, 1324–1341, https://doi.org/10.1111/j.1095-8649.1998.tb00252.x, 1998.

Kristoffersen, J. B. and Salvanes, A. G. V.: Distribution, growth, and population genetics of the glacier lanternfish (Benthosema glaciale) in Norwegian waters: Contrasting patterns in fjords and the ocean, Mar. Biol. Res., 5, 596–604, https://doi.org/10.1080/17451000903042479, 2009.

Lee, K., Kim, T.-W., Byrne, R. H., Millero, F. J., Feely, R. A., and Liu, Y.-M.: The universal ratio of boron to chlorinity for the North Pacific and North Atlantic oceans, Geochim. Cosmochim. Acta, 74, 1801–1811, https://doi.org/10.1016/j.gca.2009.12.027, 2010.

Limburg, K. E. and Casini, M.: Otolith chemistry indicates recent worsened Baltic cod condition is linked to hypoxia exposure, Biol. Lett., 15, 20190352, https://doi.org/10.1098/rsbl.2019.0352, 2019.

Limburg, K. E., Olson, C., Walther, Y., Dale, D., Slomp, C. P., and Hoie, H.: Tracking Baltic hypoxia and cod migration over millennia with natural tags, Proc. Natl. Acad. Sci., 108, E177–E182, https://doi.org/10.1073/pnas.1100684108, 2011.

Limburg, K. E., Walther, B. D., Lu, Z., Jackman, G., Mohan, J., Walther, Y., Nissling, A., Weber, P. K., and Schmitt, A. K.: In search of the dead zone: Use of otoliths for tracking fish exposure to hypoxia, J. Mar. Syst., 141, 167–178, https://doi.org/10.1016/j.jmarsys.2014.02.014, 2015.

Limburg, K. E., Wuenschel, M. J., Hüssy, K., Heimbrand, Y., and Samson, M.: Making the Otolith Magnesium Chemical Calendar-Clock Tick: Plausible Mechanism and Empirical Evidence, Rev. Fish. Sci. Aquac., 26, 479–493, https://doi.org/10.1080/23308249.2018.1458817, 2018.

Limburg, K. E., Heimbrand, Y., and Kuliński, K.: Marked recent declines in boron in Baltic Sea cod otoliths – a bellwether of incipient acidification in a vast hypoxic system?, Biogeosciences, 20, 4751–4760, https://doi.org/10.5194/bg-20-4751-2023, 2023.

Longerich, H. P., Jackson, S. E., and Günther, D.: Inter-laboratory note. Laser ablation inductively coupled plasma mass spectrometric transient signal data acquisition and analyte concentration calculation, J. Anal. At. Spectrom., 11, 899–904, https://doi.org/10.1039/JA9961100899, 1996.

Loutrage, L., Brind'Amour, A., Chouvelon, T., and Spitz, J.: Ontogenetic shift or not? Different foraging trade-offs within the meso- to bathypelagic fish community, Ecol. Evol., 14, e11129, https://doi.org/10.1002/ece3.11129, 2024.

Meyer, H. K., Roberts, E. M., Mienis, F., and Rapp, H. T.: Drivers of Megabenthic Community Structure in One of the World's Deepest Silled-Fjords, Sognefjord (Western Norway), Front. Mar. Sci., 7, https://doi.org/10.3389/fmars.2020.00393, 2020.

Mohan, J. A., Dewar, H., Snodgrass, O. E., Miller, N. R., Tanaka, Y., Ohshimo, S., Rooker, J. R., Francis, M., and Wells, R. J. D.: Otolith geochemistry reflects life histories of Pacific bluefin tuna, PLOS ONE, 17, e0275899, https://doi.org/10.1371/journal.pone.0275899, 2022.

Morales-Nin, B.: Review of the growth regulation processes of otolith daily increment formation, Fish. Res., 46, 53–67, https://doi.org/10.1016/S0165-7836(00)00133-8, 2000.

Ng, C. Z. W., Reis-Santos, P., Gonzalez, J. G., Gillanders, B. M., Saleh, M. F., and Ong, J. J. L.: A non-linear statistical framework to investigate changes in life history patterns within and among fish populations, Rev. Fish Biol. Fish., 35, 2065–2080, https://doi.org/10.1007/s11160-025-09993-0, 2025.

https://doi.org/10.5194/egusphere-2026-4521
Preprint. Discussion started: 7 August 2026

Omar, A. M., Skjelvan, I., Rune Erga, S., and Olsen, A.: Aragonite saturation states and pH in western Norwegian fjords: seasonal cycles and controlling factors, 2005-2009, Ocean Sci., 12, 937–951, https://doi.org/10.5194/os-12-937-2016, 2016.

Paetzel, M. and Dale, T.: Climate proxies for recent fjord sediments in the inner Sognefjord region, western Norway, Geol. Soc. Lond. Spec. Publ., 344, 271–288, https://doi.org/10.1144/SP344.19, 2010.

Palmer, M. R. and Edmond, J. M.: The strontium isotope budget of the modern ocean, Earth Planet. Sci. Lett., 92, 11–26, https://doi.org/10.1016/0012-821X(89)90017-4, 1989.

Paton, C., Hellstrom, J., Paul, B., Woodhead, J., and Hergt, J.: Iolite: Freeware for the visualisation and processing of mass spectrometric data, J. Anal. At. Spectrom., 26, 2508–2518, https://doi.org/10.1039/c1ja10172b., 2011.

Pedersen, E. J., Miller, D. L., Simpson, G. L., and Ross, N.: Hierarchical generalized additive models in ecology: an introduction with mgcv, PeerJ, 7, e6876, https://doi.org/10.7717/peerj.6876, 2019.

Persson, L. and Crowder, L. B.: Fish-Habitat Interactions Mediated via Ontogenetic Niche Shifts, in: The Structuring Role of Submerged Macrophytes in Lakes, edited by: Jeppesen, E., Søndergaard, M., Søndergaard, M., and Christoffersen, K., Springer, New York, NY, 3–23, https://doi.org/10.1007/978-1-4612-0695-8_1, 1998.

Proud, R., Cox, M. J., and Brierley, A. S.: Biogeography of the Global Ocean's Mesopelagic Zone, Curr. Biol. CB, 27, 113–119, https://doi.org/10.1016/J.CUB.2016.11.003, 2017.

Quintela, M., García-Seoane, E., Dahle, G., Klevjer, T. A., Melle, W., Lille-Langøy, R., Besnier, F., Tsagarakis, K., Geoffroy, M., Rodríguez-Ezpeleta, N., Jacobsen, E., Côté, D., Knutar, S., Unneland, L., Strand, E., and Glover, K.: Genetics in the Ocean's Twilight Zone: Population Structure of the Glacier Lanternfish Across Its Distribution Range, Evol. Appl., 17, e70032, https://doi.org/10.1111/EVA.70032, 2024.

Reygondeau, G., Guidi, L., Beaugrand, G., Henson, S. A., Koubbi, P., MacKenzie, B. R., Sutton, T. T., Fioroni, M., and Maury, O.: Global biogeochemical provinces of the mesopelagic zone, J. Biogeogr., 45, 500–514, https://doi.org/10.1111/jbi.13149, 2018.

Robinson, C., Steinberg, D. K., Anderson, T. R., Arístegui, J., Carlson, C. A., Frost, J. R., Ghiglione, J. F., Hernández-León, S., Jackson, G. A., Koppelmann, R., Quéguiner, B., Ragueneau, O., Rassoulzadegan, F., Robison, B. H., Tamburini, C., Tanaka, T., Wishner, K. F., and Zhang, J.: Mesopelagic zone ecology and biogeochemistry – a synthesis, Deep Sea Res. Part II Top. Stud. Oceanogr., 57, 1504–1518, https://doi.org/10.1016/J.DSR2.2010.02.018, 2010.

de Roos, A. M., Leonardsson, K., Persson, L., and Mittelbach, G. G.: Ontogenetic Niche Shifts and Flexible Behavior in Size-Structured Populations, Ecol. Monogr., 72, 271–292, https://doi.org/10.1890/0012-9615(2002)072%5B0271:ONSAFB%5D2.0.CO;2, 2002.

Saba, G. K., Burd, A. B., Dunne, J. P., Hernández-León, S., Martin, A. H., Rose, K. A., Salisbury, J., Steinberg, D. K., Trueman, C. N., Wilson, R. W., and Wilson, S. E.: Toward a better understanding of fish-based contribution to ocean carbon flux, Limnol. Oceanogr., 66, 1639–1664, https://doi.org/10.1002/lno.11709, 2021.

Saltalamacchia, F., Gallo, N. D., Limburg, K., Folkvord, A., and Salvanes, A. G. V.: Otolith shape and microchemistry reveal fine-scale population connectivity in the myctophid Benthosema glaciale (Reinhardt, 1837) along a complex seascape, Sci. Rep., 16, 18982, https://doi.org/10.1038/s41598-026-46216-3, 2026.

Salvanes, A. G. V. and Stockley, B. M.: Spatial variation of growth and gonadal developments of Maurolicus muelleri in the Norwegian Sea and in a Norwegian fjord, Mar. Biol., 126, 321–332, https://doi.org/10.1007/BF00347456, 1996.

https://doi.org/10.5194/egusphere-2026-4521
Preprint. Discussion started: 7 August 2026

Salvanes, A. G. V., Devine, J., Jensen, K. H., Hestetun, J. T., Sjøtun, K., and Glenner, H. (Editors): Marine Ecological Field Methods - A Guide for Marine Biologists and Fisheries Scientists, Wiley-Blackwell, 2018.

Salvanes, A. G. V., Gallo, N. D., Solås, M. R., Saltalamacchia, F., Aksnes, D. L., Darelius, E., Christiansen, S., Folkvord, A., Hosia, A., Kaartvedt, S., Levin, L., Limburg, K., Martell, L., Midtøy, F., Myksvoll, M., Risebrobakken, B., Savolainen, H., Skadal, J., and Staby, A.: Deep Fjords Are Excellent Natural Infrastructure for Climate Impact Studies, Fish Fish., 0, 1–8, https://doi.org/10.1111/faf.12879, 2025.

Sánchez-Hernández, J., Nunn, A. D., Adams, C. E., and Amundsen, P.-A.: Causes and consequences of ontogenetic dietary shifts: a global synthesis using fish models, Biol. Rev., 94, 539–554, https://doi.org/10.1111/brv.12468, 2019.

Schneider, C. A., Rasband, W. S., and Eliceiri, K. W.: NIH Image to ImageJ: 25 years of image analysis, Nat. Methods, 9, 671–675, https://doi.org/10.1038/nmeth.2089, 2012.

Skei, J. M. and Melsom, S.: Seasonal and vertical variations in the chemical composition of suspended particulate matter in an oxygen-deficient fjord, Estuar. Coast. Shelf Sci., 14, 61-IN1, https://doi.org/10.1016/S0302-3524(82)80067-4, 1982.

Søvik, G., Falkenhaug, T., Zimmermann, F., Gallo, N. D., Nedreaas, K., Danre, J.-B., Hovland, T., Thangstad, T. H., Olsen, S. A., Johnsen, E., and Asplin, L.: Toktrapport fra økosystemtokt i Vestlandsfjordene — Hydrografi, vannkjemi, reker, krill, bunnfisk, tobis og perifylla, Havforskningsinstituttet, 2023.

St. John, M. A., Borja, A., Chust, G., Heath, M., Grigorov, I., Mariani, P., Martin, A. P., and Santos, R. S.: A Dark Hole in Our Understanding of Marine Ecosystems and Their Services: Perspectives from the Mesopelagic Community, Front. Mar. Sci., 3, https://doi.org/10.3389/fmars.2016.00031, 2016.

Stanley, R. R. E., Bradbury, I. R., DiBacco, C., Snelgrove, P. V. R., Thorrold, S. R., and Killen, S. S.: Environmentally mediated trends in otolith composition of juvenile Atlantic cod (Gadus morhua), ICES J. Mar. Sci., 72, 2350–2363, https://doi.org/10.1093/icesjms/fsv070, 2015.

Stigebrandt, A.: Hydrodynamics and circulation of fjords, Encycl. Lakes Reserv., 327, 344, 2012.

Sturrock, A. M., Hunter, E., Milton, J. A., Johnson, R. C., Waring, C. P., Trueman, C. N., and EIMF: Quantifying physiological influences on otolith microchemistry, Methods Ecol. Evol., 6, 806–816, https://doi.org/10.1111/2041-210X.12381, 2015.

Suneetha, K. B. and Salvanes, A. G. V.: Population genetic structure of the glacier lanternfish, Benthosema glaciale (Myctophidae) in Norwegian waters, Sarsia, 86, 203–212, https://doi.org/10.1080/00364827.2001.10420476, 2001.

Syvitski, J. P., Burrell, D. C., and Skei, J. M.: Fjords: processes and products, Springer Science & Business Media, 2012.

Thorrold, S. R., Jones, C. M., and Campana, S. E.: Response of otolith microchemistry to environmental variations experienced by larval and juvenile Atlantic croaker (Micropogonias undulatus), Limnol. Oceanogr., 42, 102–111, https://doi.org/10.4319/lo.1997.42.1.0102, 1997.

Thorrold, S. R., Latkoczy, C., Swart, P. K., and Jones, C. M.: Natal Homing in a Marine Fish Metapopulation, Science, 291, 297–299, https://doi.org/10.1126/science.291.5502.297, 2001.

Turner, S. M. and Limburg, K. E.: Does Daily Growth Affect the Rate of Manganese Uptake in Juvenile River Herring Otoliths?, Trans. Am. Fish. Soc., 144, 873–881, https://doi.org/10.1080/00028487.2015.1059888, 2015.

https://doi.org/10.5194/egusphere-2026-4521
Preprint. Discussion started: 7 August 2026

Vastenhoud, B. M. J., Mildenberger, T. K., Kokkalis, A., Paoletti, S., Alvarez, P., Garcia, D., Wieczorek, A. M., Klevjer, T., Melle, W., Jonsson, S. T., and Nielsen, J. R.: Growth and natural mortality of Maurolicus muelleri and Benthosema glaciale in the Northeast Atlantic Ocean, Front. Mar. Sci., 10, 1278778, https://doi.org/10.3389/fmars.2023.1278778, 2023.

Vestheim, H., Røstad, A., Klevjer, T. A., Solberg, I., and Kaartvedt, S.: Vertical distribution and diel vertical migration of krill beneath snow-covered ice and in ice-free waters, J. Plankton Res., 36, 503–512, https://doi.org/10.1093/plankt/fbt112, 2014.

Vrdoljak, D., Matić-Skoko, S., Peharda, M., Uvanović, H., Markulin, K., and Mertz-Kraus, R.: Otolith fingerprints reveals potential pollution exposure of newly settled juvenile *Sparus aurata*, Mar. Pollut. Bull., 160, 111695, https://doi.org/10.1016/j.marpolbul.2020.111695, 2020.

Walther, B. D. and Limburg, K. E.: The use of otolith chemistry to characterize diadromous migrations, J. Fish Biol., 81, 796–825, https://doi.org/10.1111/J.1095-8649.2012.03371.X, 2012.

Walther, B. D., Kingsford, M. J., and McCulloch, M. T.: Environmental Records from Great Barrier Reef Corals: Inshore versus Offshore Drivers, PLOS ONE, 8, e77091, https://doi.org/10.1371/journal.pone.0077091, 2013.

Wood, S. N.: mgcv: GAMs and generalized ridge regression for R, R News, 1, 20–25, 2001.

Wu, L., Zhuang, W., Liu, Q., Wang, R., Li, Y., Lin, L., Liu, S., and Ding, S.: Pilot study to reconstruct life history of Diaphus thiollierei from the Arabian Sea by otolith microstructure and microchemistry, Acta Oceanol. Sin., 43, 75–84, https://doi.org/10.1007/s13131-024-2307-x, 2024.

Xuan, Z., Wang, X., Hajisamae, S., Tsim, K. W. K., Yang, J., and Wang, W.-X.: Otolith microchemistry reveals different environmental histories for two endangered fourfinger threadfin species, Mar. Ecol. Prog. Ser., 700, 161–178, https://doi.org/10.3354/meps14187, 2022.

Yu, J., Elderfield, H., and Hönisch, B.: B/Ca in planktonic foraminifera as a proxy for surface seawater pH, Paleoceanography, 22, https://doi.org/10.1029/2006PA001347, 2007.